Turbulent dispersion from line sources in grid turbulence

Sharadha Viswanathan and Stephen B. Pope
Sibley School of Mechanical and Aerospace Engineering, Cornell University, Ithaca, New York 14853, USA

(Received 1 January 2008; accepted 6 April 2008; published online 31 October 2008)

Probability density function (PDF) calculations are reported for the dispersion from line sources in decaying grid turbulence. The calculations are performed using a modified form of the interaction by exchange with the conditional mean (IECM) mixing model. These flows pose a significant challenge to statistical models because the scalar length scale (of the initial plume) is much smaller than the turbulence integral scale. Consequently, this necessitates incorporating the effects of molecular diffusion in order to model laboratory experiments. Previously, Sawford [Flow Turb. Combust. **72**, 133 (2004)] performed PDF calculations in conjunction with the IECM mixing model, modeling the effects of molecular diffusion as a random walk in physical space and using a mixing time scale empirically fit to the experimental data of Warhaft [J. Fluid Mech. **144**, 363 (1984)]. The resulting transport equation for the scalar variance contains a spurious production term. In the present work, the effects of molecular diffusion are instead modeled by adding a conditional mean scalar drift term, thus avoiding the spurious production of scalar variance. A laminar wake model is used to obtain an analytic expression for the mixing time scale at small times, and this is used as part of a general specification of the mixing time scale. Based on this modeling, PDF calculations are performed, and comparison is made primarily with the experimental data of Warhaft on single and multiple line sources and with the previous calculations of Sawford. A heated mandoline is also considered with comparison to the experimental data of Warhaft and Lumley [J. Fluid Mech. **88**, 659 (1978)]. This establishes the validity of the proposed model and the significant effect of molecular diffusion on the decay of scalar fluctuations. The following are the significant predictions of the model. For the line source, the effect of the source size is limited to early times and can be completely accounted for by simple transformations. The peak centerline ratio of the rms to the mean of the scalar increases with the Reynolds number (approximately as $R_\lambda^{1/3}$), whereas this ratio tends to a constant (approximately 0.4) at large times independent of R_λ. In addition, the model yields a universal long-time decay exponent for the temperature variance. © *2008 American Institute of Physics*. [DOI: 10.1063/1.3006069]

I. INTRODUCTION

Turbulent mixing and dispersion of passive scalars are of enormous interest in order to understand various phenomena such as combustion and pollutant dispersion and is a well researched area. The earliest theoretical studies of turbulent diffusion were performed by Taylor[1,2] in his theory of diffusion by continuous movements for self-preserving turbulence. Following his study, a large number of laboratory wind tunnel measurements of diffusion of heat in the thermal wake behind heated line elements were performed.[3–7]

In particular, Stapountzis *et al.*[5] analyzed the structure and development of the heated plume behind a single line source in homogeneous turbulence experimentally and theoretically using displacement statistics between pairs of particles, and they noted that the meandering of the thermal wake is the dominant reason for the thermal fluctuations close to the source. Warhaft[7] performed a detailed study of the wake behind a single line source and proceeded to analyze the interference between pairs of line sources using the inference method elaborated in Ref. 8 and also noted that a heated *mandoline* can be obtained by superimposing a number of such line sources.

On the modeling side, for chemically inert flows, probability density function (PDF) methods based on the velocity-scalar joint PDF[9–12] have been proposed. PDF methods yield the convection terms in closed form while the conditional acceleration and conditional scalar dissipation need to be modeled. The Langevin equation is one among the many stochastic models proposed as a closure for the conditional acceleration term. In order to close the conditional scalar dissipation term, various mixing models have been proposed. In the context of chemical reactor engineering, the interaction by exchange with the mean (IEM) model was postulated by Villermaux and Devillon.[13] Dopazo and O'Brien[14] introduced an identical model in the context of the composition PDF equation in homogeneous turbulence but referred to it as the linear mean-square estimation model (LMSE).

These models were originally proposed for statistically homogeneous situations, and for inhomogeneous flows they are implemented so as to be local in physical space. The question of the connection between scalar mixing and velocity arises when the joint velocity-scalar PDF is considered.

Pope[15] analyzed the modeling provided by the Langevin equation for velocity combined with Curl's[16] mixing model for composition. His analysis showed that in isotropic turbulence, the predicted decay rate of the velocity-composition

correlation coefficient is substantially larger than that observed experimentally. It was also shown that if the scalar mixing is biased toward fluid having similar velocities, then the decay rate of the scalar flux is reduced to be within the experimental range. A velocity-biased mixing model based on these ideas was developed by Song.[17]

Pope[18] observed that the combination of the Langevin equation and IEM model implies that there is dissipation of the scalar flux and that this is inconsistent with local isotropy. It was observed that this inconsistency is avoided if, in the IEM model, the mean composition is replaced by its mean conditioned on velocity. Although its name arose later, this results in the interaction by exchange with the conditional mean (IECM) mixing model [Eq. (1)]. In the IECM mixing model, the particle's composition $\phi(t)$ relaxes to the local conditional mean according to

$$\frac{d\phi}{dt} = -\omega_m(\phi - \langle\phi|\mathbf{u},\mathbf{x}\rangle), \tag{1}$$

where ω_m is the mixing rate (the inverse of the mixing time scale t_m), $\mathbf{u}$ and $\mathbf{x}$ are the particle's velocity and position, and $\langle\phi|\mathbf{u},\mathbf{x}\rangle$ denotes the mean composition at $\mathbf{x}$ conditioned on the velocity being $\mathbf{u}$.

Fox[19] introduced the "velocity-conditioned IEM" model in which the composition relaxes to

$$\zeta\langle\phi\rangle + (1-\zeta)\langle\phi|\mathbf{u},\mathbf{x}\rangle \tag{2}$$

for $0 \le \zeta \le 1$. For $\zeta=1$ and $\zeta=0$, this corresponds to the IEM and the IECM model, respectively. The direct numerical simulation (DNS) data of Overholt and Pope[20] were used to show that ζ decreases toward zero with increasing the Reynolds number, consistent with local isotropy. The vanishing effect of molecular diffusivity on the scalar flux was considered further by Pope,[21] and apparently in this paper, the name "IECM" is introduced.

A decade earlier, Anand and Pope[22] applied a velocity-composition PDF model to the problem of dispersion from a line source in grid turbulence using a combination of the Langevin equation and the IEM model. With the standard (unconditional) application of the model, the scalar variance greatly exceeds the observed levels. The model was also applied conditioning the scalar mean on the velocity at the source. Close to the source (i.e., for flight times small compared to the Lagrangian integral time scale) the fluid velocity changes little from the value at the source and hence, this conditional model is very similar to the IECM mixing model (in this region). With the conditional model, Anand and Pope[22] were able to match the scalar variance with the experimental data to within a factor of 2 and also proposed a theory that completely predicts the evolution of the mean scalar profile.

Recently, PDF calculations modeling the dispersion behind single and pairs of line sources in decaying turbulence in conjunction with the IECM mixing model were performed by Sawford[23] by using a mixing rate empirically determined to match the experimental data. In that paper, the velocity-conditioned scalar mean for the specific case of line sources is also obtained analytically using the backward diffusion of particles.

Other modeling studies that use the IECM model include the work by Luhar and Sawford[24] where they studied the dispersion behind line and point sources in inhomogeneous non-Gaussian turbulence in convective boundary layers using a mixing rate that is fit empirically. Sawford[25] also used the IECM mixing model with the same mixing rate as in Ref. 23 to analyze the conditional scalar statistics for a line plume in turbulent channel flow comparing against the DNS data of Brethouwer and Nieuswstadt.[26]

In order to use the IECM model for a general flow problem, the mixing rate has to be specified. It is common practice to model the mixing time scale to be proportional to the turbulence time scale. DNS studies of homogeneous turbulence mixing[20,27,28] have shown that the mechanical-to-scalar time scale ratio eventually approaches a constant value independent of initial conditions. This appears, however, to be at variance with the heated mandoline experiments of Warhaft and Lumley[6] which do not suggest the relaxation of this ratio to an equilibrium value over a period of one turbulence decay time. On the other hand, Sreenivasan *et al.*[29] found a universal decay exponent for temperature fluctuations from a mandoline but a different exponent for a heated grid. Hence, the long-time behavior of the mechanical-to-scalar time scale ratio requires further study.

Due to the disparity in the length scales of the initial plume and the turbulence length scale, meandering of the instantaneous plume and the effects of molecular diffusion (in comparison to turbulent diffusion) are dominant[5,30–32] in the early stages of the plume development. Conditioning on velocity largely accounts for the fluctuations arising from meandering close to the source, but fluctuations relative to the conditional mean also develop. The IECM mixing model tends to reduce the fluctuations about the conditional mean without affecting the conditional mean itself.

The effects of molecular diffusion are twofold: transport of the scalar in physical space and mixing in the scalar space. Conventionally, the molecular transport has been modeled by a random walk in physical space[22,23] but this results in a spurious production term in the scalar variance transport equation. In the context of filtered density function methods, McDermott and Pope[33] modeled the molecular transport by a mean drift term in the scalar evolution equation and the resulting variance equation does not contain spurious production terms.

In the present work, PDF calculations are performed for single and multiple line sources in decaying grid turbulence using a modified IECM mixing model with the effects of molecular diffusion incorporated directly in the mixing model itself. The results of the calculations are compared with the experimental data of Warhaft,[7] the data of Sawford and Tivendale reported by Sawford,[23] and the recent calculations of Sawford.[23] An array of line sources is also considered with comparison to the experimental data of Warhaft and Lumley.[6] In this paper, the authors suggest that the passive scalar variance decay rate is uniquely determined by the wavenumber of the initial scalar fluctuations relative to the

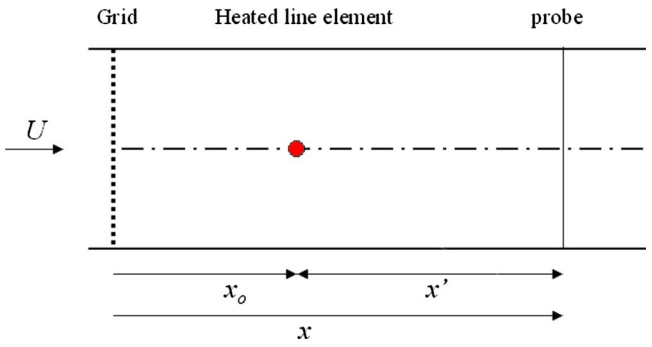

FIG. 1. (Color online) Sketch of the experimental setup showing the wind tunnel. The source (dot) is at a distance x_o from the turbulence generating grid.

turbulence integral length scale. On the other hand, Sreenivasan *et al.*[29] found that the decay rate of scalar fluctuations from an array of line sources is independent of the initial conditions.

The rest of the paper is organized as follows. Section II describes the experimental setup and relevant parameters. Section III gives a brief overview of the modeling and analysis behind the present work. The implementation details are covered in Sec. IV. Section V presents the model calculations and results along with appropriate discussions for a single line source, a pair of line sources, and an array of line sources. The final section, Sec. VI, summarizes the important conclusions.

II. EXPERIMENTAL DETAILS

A sketch of the experimental setup for a single line source in grid turbulence is shown in Fig. 1. The turbulence generating grid is taken to be the origin for the downstream distance x. The flow is in the x direction, as shown in Fig. 1, with a mean speed U. A fine heated wire forming a thermal line source is placed normal to the direction of the mean flow at a distance of x_o from the turbulence generating grid. The z direction is taken parallel to the thermal line source and y is taken to be the third normal direction. The source size is sufficiently small that it does not affect the velocity field and the temperature excess produced by the source heating soon falls to within a few degrees of the mean flow temperature. As a result, the excess temperature is a conserved passive scalar except in the near vicinity of the heated line element. We are interested in understanding the diffusion and mixing of the passive scalar in the wake behind the line source. In particular, we are interested in the scalar mean and variance profiles downstream of the source.

The velocity fluctuations u, v, and w are taken to be in the direction of the mean flow, perpendicular to the source, and parallel to the source, respectively. The velocity variance decays according to the power law given by

$$\sigma_\alpha^2(x) = \sigma_\alpha^2(M)\left(\frac{x}{M}\right)^{-m}, \tag{3}$$

where $\alpha = u, v, w$. The grid mesh spacing is given by M and m is the velocity variance decay exponent. Following Sawford,[23] the transverse velocity variance data of Warhaft have been refitted with a decay exponent of $m=1.4$ to facilitate modeling.

TABLE I. Parameters in the laboratory measurements for diffusion behind a single line source in grid turbulence (Ref. 7), effective source size σ_o, mesh spacing M, position of the source with respect to the grid, x_o/M, mean speed U, velocity standard deviation at one mesh length from the grid, $\sigma_w, \sigma_u, \sigma_v$, velocity variance decay exponent m, and molecular diffusivity κ.

σ_o	1.27×10^{-4}	m
	2.5×10^{-5}	m
M	2.54×10^{-2}	m
x_o/M	20, 52, 60	
U	7	ms^{-1}
σ_u	2.44	ms^{-1}
σ_w, σ_v	2.27	ms^{-1}
m	1.4	
κ	2.1×10^{-5}	$m^2\ s^{-1}$

The physical parameters relevant to the laboratory measurements of Warhaft[7] are consolidated in Table I.

III. MODELING

A. Turbulence

In the laboratory frame of reference, the line source is placed at a distance x_o from the turbulence grid. One-point statistics depend solely on x and y and are measured by a stationary probe positioned at various distances downstream of the source. In the reference frame moving with the mean flow, to an excellent approximation, the line source appears as an initial plane area source, and the flow evolves in time. The time t in the moving frame is related to streamwise position x in the laboratory frame by

$$x(t) = x_o + Ut. \tag{4}$$

Consequently, with Taylor's hypothesis, only the dispersion perpendicular to this area source is relevant. Thus, in this frame, one-point statistics depend solely on y and t. While the measurements are naturally made in the laboratory frame, it is most convenient to perform the modeling in the moving frame.

For decaying grid turbulence, the rate of decay of the velocity variance [Eq. (3)] can be re-expressed as a function of travel time from the source as

$$\sigma_\alpha^2(t) = \sigma_\alpha^2(0)\left(1 + \frac{t}{t_o}\right)^{-m}, \quad \alpha = u, v, w, \tag{5}$$

where t_o is the flight time to the source. Using Eq. (5), the turbulent kinetic energy $k(t)$ and the turbulent dissipation $\varepsilon(t)$ can therefore be obtained as

$$k(t) = \tfrac{1}{2}[\sigma_u^2(t) + \sigma_v^2(t) + \sigma_w^2(t)], \tag{6}$$

$$\varepsilon(t) = -\frac{d}{dt}k(t). \tag{7}$$

In the Lagrangian PDF modeling framework, the turbulent flow is represented by a large number of particles, all of which are considered to be statistically identical. Each par-

ticle carries a set of properties—velocity $v(t)$, position $y(t)$, and scalar $\phi(t)$. Stochastic models are constructed to evolve each of the particle's properties in time. The Langevin equation is one of the typical stochastic models used to model the velocity of the particle following the fluid. Conventionally, to model the position $y(t)$, the evolution equation for fluid particle velocity $dy/dt=v$ is augmented by a random term to account for molecular diffusion. Hence $y(t)$ is a model for the position of a molecule and evolves as

$$dy = v dt + \sqrt{2\kappa} dW_1, \tag{8}$$

where $W_1(t)$ is a Wiener process and κ is the molecular diffusivity. In the present work, the position $y(t)$ is instead modeled as

$$\frac{dy}{dt} = v, \tag{9}$$

and the effects of molecular diffusion are directly incorporated into the mixing model, the details of which are elaborated in Sec. III B. While the present model uses Eq. (9), the analysis in this section considers both Eqs. (8) and (9). In both cases the model for $v(t)$ is that for the velocity following a fluid particle (i.e., additional effects due to molecular motion[34] are neglected) and is

$$\begin{aligned} dv &= A(v,t)dt + \sqrt{C_0 \varepsilon} dW \\ &= -\left(\frac{1}{2} + \frac{3}{4} C_0\right) \frac{\varepsilon}{k} v dt + \sqrt{C_0 \varepsilon} dW, \end{aligned} \tag{10}$$

where $A(v,t)$ is the drift term and $W(t)$ is a second Wiener process [independent of $W_1(t)$]. We use the standard value of 2.1 for the Langevin equation model constant[35] C_0 in all our calculations unless otherwise specified.

Single particle displacement statistics can be used to obtain the mean scalar field. Hence the displacement of a particle from a location at the source at the initial time, defined as $\Delta y(t)=y(t)-y(0)$, can be related to the evolution of the mean scalar profile, which is a Gaussian field with characteristic width σ_p centered on the plume centerline. Taking into account the effect of the source size σ_o on the evolution of the plume width, σ_p can be written as

$$\sigma_p^2 = \sigma_o^2 + \sigma_y^2, \tag{11}$$

where $\sigma_y^2=\langle \Delta y^2 \rangle$ is the mean-square displacement. Anand and Pope[22] derived σ_y^2 analytically from Eqs. (8) and (10) to be

$$\sigma_y^2 = 2\kappa t + \Delta_o^2, \tag{12}$$

where the contribution from turbulent dispersion, Δ_o^2, is given by

$$\Delta_o^2 = 2\sigma_v^2(t_o) t_o^2 \left[\frac{(1+t/t_o)^{r-s}}{r(r-s)} + \frac{(1+t/t_o)^{-s}}{rs} - \frac{1}{s(r-s)} \right], \tag{13}$$

with r and s being

$$r = \frac{m}{2}\left(\frac{3}{2}C_0 - 1\right) + 1, \tag{14}$$

$$s = \frac{m}{2}\left(\frac{3}{2}C_0 + 1\right) - 1. \tag{15}$$

B. Mixing model

Various mixing models have been proposed[13–19,21] as a closure for the conditional scalar dissipation term in the velocity-scalar joint PDF transport equation. The simplest of these is the IEM model.[13,14] With the IEM mixing model, the particle's composition $\phi(t)$ relaxes to the local mean as

$$\frac{d\phi}{dt} = -\omega_m(\phi - \langle \phi | \mathbf{x} \rangle), \tag{16}$$

where $\mathbf{x}$ is the particle's position, $\langle \phi | \mathbf{x} \rangle$ is the mean composition at $\mathbf{x}$, and ω_m is the mixing rate given by

$$\omega_m = \frac{C_\phi \varepsilon}{2k}, \tag{17}$$

with $C_\phi \sim 1.2–3$.[36] The IEM model makes an unjustifiable assumption regarding the independence of the scalar mixing term with the velocity field and is inconsistent with local isotropy. On the other hand, conditioning the scalar mean on velocity is consistent with local isotropy and hence corrects the deficiency of the IEM model by performing mixing locally in velocity-physical space.

For a Lagrangian PDF calculation, the Langevin equation coupled with a mixing model comprise a set of stochastic differential equations for velocity, displacement, and scalar carried by a particle, from which the transport equation for the Lagrangian joint PDF of velocity and scalar can be derived. The various moment conservation equations can be obtained from the joint PDF transport equation.

1. IECM mixing model

In this subsection we consider the IECM mixing model as used by Sawford[23] in which the direct effects of molecular diffusivity are modeled by a random walk in position [Eq. (8)]. Then in the following subsection (Sec. III B 2) we consider the modified IECM model which instead uses Eq. (9) and the direct effects of molecular diffusion are accounted for differently [by Eq. (37), below]. The analysis shows that the two models yield the same behavior for the mean, $\langle \phi | y \rangle$, and the conditional mean, $\langle \phi | V, y \rangle$, but a different behavior for the variance, $\langle \phi'^2 \rangle$.

With the IECM mixing model as used by Sawford,[23] the transport equation for the joint PDF of velocity, scalar, and position, $\tilde{f}(V,\psi,y;t)$, and the joint PDF of velocity and position, $\tilde{g}(V,y;t)$, can be derived from Eqs. (1), (8), and (10), in which the molecular transport is modeled as a random term in the position equation. Here, V and ψ refer to the velocity and scalar sample space variables, respectively. The transport equations for $\tilde{f}$ and $\tilde{g}$ are given by

$$\frac{\partial \tilde{f}}{\partial t}+\frac{\partial V\tilde{f}}{\partial y}+\frac{\partial A(V)\tilde{f}}{\partial V}+\frac{\partial \Phi(V,\psi,y)\tilde{f}}{\partial \psi}=\kappa\frac{\partial^2\tilde{f}}{\partial y^2}+\frac{1}{2}C_0\varepsilon\frac{\partial^2\tilde{f}}{\partial V^2} \tag{18}$$

and

$$\frac{\partial \tilde{g}}{\partial t}+\frac{\partial V\tilde{g}}{\partial y}+\frac{\partial A(V)\tilde{g}}{\partial V}=\kappa\frac{\partial^2\tilde{g}}{\partial y^2}+\frac{1}{2}C_0\varepsilon\frac{\partial^2\tilde{g}}{\partial V^2}, \tag{19}$$

where $\Phi(V,\psi,y)=-\omega_m(t)(\psi-\langle\phi|V,y\rangle)$. Note that the coefficients in Eqs. (18) and (19) depend on time.

From Eq. (18), transport equations for the different moments of the scalar can be obtained. In particular, the transport equations for the mean [Eq. (20)] and the mean square [Eq. (31)] of the scalar are of interest. Multiplying Eq. (18) by ψ and integrating over the (ψ,V) sample space, we obtain the transport equation for $\langle\phi\rangle$ to be

$$\frac{\partial\langle\phi\rangle}{\partial t}+\frac{\partial\langle v\phi\rangle}{\partial y}=\kappa\frac{\partial^2\langle\phi\rangle}{\partial y^2}, \tag{20}$$

which is identical to the exact conservation equation. The IECM mixing model does not affect the mean scalar field as all the moments first-order in ϕ are unaffected by mixing:

$$\langle\nu^n\Phi(\phi)\rangle=0, \quad n=0,1,2,\ldots. \tag{21}$$

Therefore, single particle displacement statistics can be used to obtain the mean scalar field. Hence, the square of the mean plume width σ_p is given by Eq. (11) as the sum of σ_o^2 and the particle displacement variance σ_y^2.

Likewise, the transport equation for the conditional mean, $\tilde{c}=\langle\phi|V,y\rangle$, can be obtained from Eqs. (18) and (19) based on its definition,

$$\int_0^\infty \psi\tilde{f}(V,\psi,y)d\psi=\tilde{c}\tilde{g}(V,y), \tag{22}$$

as

$$\frac{\partial\tilde{c}}{\partial t}+V\frac{\partial\tilde{c}}{\partial y}+A\frac{\partial\tilde{c}}{\partial V}=\kappa\frac{\partial^2\tilde{c}}{\partial y^2}+\frac{1}{2}C_0\varepsilon\frac{\partial^2\tilde{c}}{\partial V^2}+C_o\varepsilon\frac{\partial\ln\tilde{g}}{\partial V}\frac{\partial\tilde{c}}{\partial V}+\kappa\frac{\partial\ln\tilde{g}}{\partial y}\frac{\partial\tilde{c}}{\partial y}. \tag{23}$$

Since the conditional mean is also unaffected by mixing with the IECM model, its transport equation can be obtained from the displacement statistics[23] (in other words, $\tilde{g}$) and the source condition is effected by considering particles that cross the source at the initial time and hence, $\partial g/\partial y$ is nonzero. For the case of a single line source of strength Q in grid turbulence, one obtains

$$\langle\phi|V,y\rangle=\frac{Q}{\sqrt{2\pi}\tilde{\sigma}}\exp\left[-\frac{1}{2}\left(\frac{y-\tilde{y}}{\tilde{\sigma}}\right)^2\right], \tag{24}$$

where the conditional center $\tilde{y}(V,t)$ is

$$\tilde{y}=\rho_{vy}V\sigma_y/\sigma_v \tag{25}$$

and the width $\tilde{\sigma}(t)$ is

$$\tilde{\sigma}=\sqrt{\sigma_o^2+\sigma_y^2(1-\rho_{vy}^2)}. \tag{26}$$

Here $\rho_{vy}(t)=\langle v\Delta y\rangle/\sigma_y\sigma_v$ is defined to be the correlation coefficient between the velocity and displacement from the source and is given by

$$\rho_{vy}=\frac{1}{\sigma_v\sigma_y}\frac{\sigma_v^2(t_o)t_o}{r}[(1+t/t_o)^{r-s-1}-(1+t/t_o)^{-s-1}]. \tag{27}$$

The conditional mean can also be obtained by solving Eq. (23) with the appropriate initial condition on $\tilde{c}$. In this case, all particles that are initially distributed in the physical domain are considered and $\partial g/\partial y$ becomes zero. It has been verified that, consistently, this procedure also yields solution Eq. (24).

With ϕ' being the fluctuation in ϕ about its mean, the transport equation for the scalar flux $\langle v\phi'\rangle$ can be obtained from Eq. (18) by multiplying by $V\psi$ and integrating:

$$\frac{\partial}{\partial t}\langle v\phi'\rangle+\frac{\partial}{\partial y}\langle v^2\phi\rangle=\langle A\phi\rangle+\langle v\Phi\rangle+\kappa\frac{\partial^2}{\partial y^2}\langle v\phi'\rangle. \tag{28}$$

A consequence of local isotropy of the velocity and scalar fields is that $\langle v\Phi\rangle$ is zero. For the IEM model we obtain instead

$$\langle v\Phi\rangle=-\omega_m\langle v(\phi-\langle\phi\rangle)\rangle=-\omega_m\langle v\phi'\rangle\neq 0, \tag{29}$$

while with the IECM model the contribution from the mixing term is

$$\langle v\Phi\rangle=-\omega_m\langle v(\phi-\langle\phi|v\rangle)\rangle=0. \tag{30}$$

Similarly, the transport equation for the mean square of the scalar can be obtained by multiplying the joint PDF transport equation, Eq. (18), by ψ^2 and integrating over the entire (ψ,V) sample space, which yields

$$\frac{\partial\langle\phi^2\rangle}{\partial t}+\frac{\partial\langle v\phi^2\rangle}{\partial y}=\kappa\frac{\partial^2\langle\phi^2\rangle}{\partial y^2}-2\omega_m\Theta, \tag{31}$$

where Θ is defined by Eq. (33). The modeled scalar variance transport equation can be obtained from Eqs. (20) and (31) as

$$\frac{\partial\langle\phi'^2\rangle}{\partial t}+2\langle v\phi'\rangle\frac{\partial\langle\phi\rangle}{\partial y}+\frac{\partial\langle v\phi'^2\rangle}{\partial y}=\kappa\frac{\partial^2\langle\phi'^2\rangle}{\partial y^2}+2\kappa\left(\frac{\partial\langle\phi\rangle}{\partial y}\right)^2-2\omega_m\Theta, \tag{32}$$

where evidently

$$2\omega_m\Theta=2\omega_m(\langle\phi^2\rangle-\langle\tilde{c}^2\rangle) \tag{33}$$

is the scalar variance dissipation according to the IECM model. Comparing the IECM model scalar variance transport equation given by Eq. (32) against the exact scalar variance transport equation,

$$\frac{\partial\langle\phi'^2\rangle}{\partial t}+2\langle v\phi'\rangle\frac{\partial\langle\phi\rangle}{\partial y}+\frac{\partial\langle v\phi'^2\rangle}{\partial y}=\kappa\frac{\partial^2\langle\phi'^2\rangle}{\partial y^2}-2\kappa\left\langle\frac{\partial\phi'}{\partial x_i}\frac{\partial\phi'}{\partial x_i}\right\rangle, \tag{34}$$

it is apparent that the modeled scalar variance transport equa-

tion gives rise to a spurious production term $\mathcal{P}$ given by

$$\mathcal{P} = 2\kappa\left(\frac{\partial\langle\phi\rangle}{\partial y}\right)^2. \tag{35}$$

2. Modified IECM mixing model

In order to eliminate the spurious production term in the scalar variance transport equation, in the present model, diffusion is removed from the position equation [i.e., Eq. (9) is used in place of Eq. (8)], and the effects of molecular diffusion are directly incorporated into the mixing model along lines similar to McDermott and Pope.[33] The molecular diffusion is modeled into the IECM mixing model by the addition of a conditional mean scalar drift term, $H(\mathbf{u},\mathbf{x})$, defined as

$$H(\mathbf{u},\mathbf{x}) = \kappa\nabla^2\langle\phi|\mathbf{u},\mathbf{x}\rangle, \tag{36}$$

to obtain the modified IECM mixing model,

$$\frac{d\phi}{dt} = H(\mathbf{u},\mathbf{x}) - \omega_m(\phi - \langle\phi|\mathbf{u},\mathbf{x}\rangle). \tag{37}$$

The transport equations for the joint PDF of position, velocity, and scalar, $f(V,\psi,y;t)$, and the joint PDF of position and velocity, $g(V,y;t)$, can be derived from Eqs. (9), (10), and (37) as

$$\frac{\partial f}{\partial t} + \frac{\partial Vf}{\partial y} + \frac{\partial A(V)f}{\partial V} + \frac{\partial H(V,y)f}{\partial\psi} + \frac{\partial\Phi(V,y,\psi)f}{\partial\psi} = \frac{1}{2}C_0\varepsilon\frac{\partial^2 f}{\partial V^2} \tag{38}$$

and

$$\frac{\partial g}{\partial t} + \frac{\partial Vg}{\partial y} + \frac{\partial A(V)g}{\partial V} = \frac{1}{2}C_0\varepsilon\frac{\partial^2 g}{\partial V^2}, \tag{39}$$

respectively. Note that we distinguish between the PDFs f and g according to the modified IECM model and the corresponding PDFs $\tilde{f}$ and $\tilde{g}$ according to the original IECM model. The evolution equation for f, Eq. (38), contains the term in H, which is absent from Eq. (18) for $\tilde{f}$, whereas Eq. (19) for $\tilde{g}$ contains the term in κ which is absent from Eq. (39) for g.

It is important to observe that the evolution equations for the mean $\langle\phi\rangle$ and the scalar flux $\langle v\phi'\rangle$ derived from Eqs. (38) and (39) agree with Eqs. (20) and (28), respectively, and so the two model variants yield identical fields of $\langle\phi\rangle$ and $\langle v\phi'\rangle$.

The scalar variance transport equation derived from Eqs. (38) and (39) contains no production terms and can be written as

$$\frac{\partial\langle\phi'^2\rangle}{\partial t} + 2\langle v\phi'\rangle\frac{\partial\langle\phi\rangle}{\partial y} + \frac{\partial\langle v\phi'^2\rangle}{\partial y} = 2\kappa\left[\left\langle c\frac{\partial^2 c}{\partial y^2}\right\rangle - \langle\phi\rangle\frac{\partial^2\langle\phi\rangle}{\partial y^2}\right] - 2\omega_m[\langle\phi^2\rangle - \langle c^2\rangle], \tag{40}$$

where $c = \langle\phi|V,y\rangle$ is the conditional scalar mean. (Note that we distinguish between the conditional means $\tilde{c}$ and c given by the two model variants.) The transport equation for the conditional scalar mean can be obtained from Eqs. (38) and (39) as

$$\frac{\partial c}{\partial t} + \frac{\partial Vc}{\partial y} + A\frac{\partial c}{\partial V} = \kappa\frac{\partial^2 c}{\partial y^2} + \frac{1}{2}C_0\varepsilon\frac{\partial^2 c}{\partial V^2} + C_o\varepsilon\frac{\partial\ln g}{\partial V}\frac{\partial c}{\partial V}. \tag{41}$$

Comparing Eq. (41) with Eq. (23), we observe that Eq. (41) is of the same form as Eq. (23) except for the omission of the term in $\partial\ln\tilde{g}/\partial y$. The modified IECM mixing model affects the evolution of the conditional mean through the term $\kappa\partial^2 c/\partial y^2$, and therefore displacement statistics cannot be used to obtain the conditional mean analytically. Since Eq. (41) is linear in c, it admits a Gaussian solution with an initial condition, $c = \langle\phi\rangle_{t=0}$, and can be solved for. On the other hand, for the line source, the source condition is effected by the initial condition on the conditional mean and hence, the term $\partial g/\partial y$ becomes zero, reducing Eq. (23) to Eq. (41), implying that $\tilde{c} = c$ for identical initial conditions.

In summary, the two variants of the IECM model lead to identical results for the mean $\langle\phi\rangle$, the conditional mean $\langle\phi|V,y\rangle$, and the scalar flux $\langle v\phi'\rangle$. However, the variance

TABLE II. Characteristics of the velocity field corresponding to the parameters in Table I; effective source size σ_o, source position relative to the grid, x_o/M, Kolmogorov length scale η, turbulence length scale L, integral scale Reynolds number, $R_L = k_o^2/\varepsilon_o^2\nu$, and Taylor scale Reynolds number $R_\lambda = \sqrt{(20/3)R_L}$ at the source.

σ_o	1.27×10^{-4}	2.5×10^{-5}		(m)
x_o/M	20	52	60	
η	1.99×10^{-4}	3.53×10^{-4}	3.84×10^{-4}	(m)
L	1.02×10^{-2}	1.35×10^{-2}	1.43×10^{-2}	(m)
R_L	431	294	278	
R_λ	54	44	43	

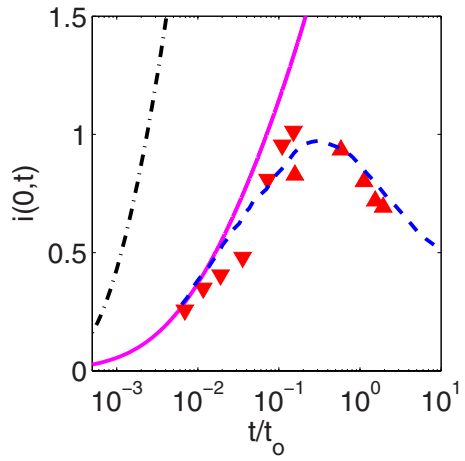

FIG. 2. (Color online) Comparison of the centerline intensity of fluctuations obtained using the laminar thermal wake model: $\kappa=0$ (dot-dashed line) and $\kappa=2.1\times10^{-5}$ m^2 s^{-1} (solid line); Warhaft (Ref. 7) data (▼) and Warhaft (Ref. 7) data $\sigma_o=1.27\times10^{-4}$ m (▲); Sawford's (Ref. 23) model calculations (dashed line) plotted against flight time from the source for source position $x_o/M=52$ and source size $\sigma_o=2.5\times10^{-5}$ m.

$\langle \phi'^2 \rangle$ evolves differently [as revealed by the right-hand sides of Eqs. (32) and (40)]. Most importantly, the modified IECM model avoids the spurious production term $\mathcal{P}$.[37]

C. Laminar thermal wake modeling

There are three relevant length scales in the passive scalar diffusion behind a line source: the instantaneous plume width σ_p, the Kolmogorov length scale η, and the turbulence integral length scale L. The relative magnitudes of the three length scales are summarized in Table II. The source is sufficiently small so as not to affect the underlying velocity field, and it is comparable to the Kolmogorov length scale at the source location. For such small sources with $\sigma_o/L \ll 1$, one of the dominating factors that influence the evolution of the scalar variance in the vicinity of the source is the molecular diffusivity.[30] In addition to the direct effect of molecular processes, the instantaneous plume is affected by the velocity at the source at the initial time.[22]

Very close to the source, the scalar field can therefore be locally modeled as evolving due to molecular diffusion in a constant and uniform velocity field, given by the velocity at the source at the initial time, v_o. The instantaneous scalar field can thus be modeled as a Gaussian of width $\sqrt{\sigma_o^2+2\kappa t}$ convected by a distance $v_o t$. As a consequence, for a fluid particle with position $y(t)$ and velocity $v(t)$, the scalar carried by the particle is (according to this model at early time) given by

$$\phi(y,v;t) = \frac{Q}{\sqrt{2\pi}\bar{\sigma}} \exp\left[-\frac{1}{2}\left(\frac{y-vt}{\bar{\sigma}} \right)^2 \right], \tag{42}$$

where the thermal wake thickness $\bar{\sigma}(t)$ is

$$\bar{\sigma} = \sqrt{\sigma_o^2 + 2\kappa t}. \tag{43}$$

Thus, the effects of both the molecular diffusion (on the plume width) and the randomness in v_o (on the plume meandering) are accounted for. To evaluate the correctness of the model, the centerline intensity of fluctuations $i(0,t) = \langle \phi'^2 \rangle_{y=0}^{1/2} / \langle \phi \rangle_{y=0}$ is compared to the experimental data and model calculations by Sawford[23] in Fig. 2. Including the effects of molecular diffusion in modeling the plume as a laminar thermal wake close to the source gives good agreement with the other two data sets in the initial stages of the plume development. However, as may be seen, ignoring molecular diffusion grossly overpredicts the scalar variance. From Fig. 2, it can also be inferred that, as expected, this model is valid only in the initial stages of the plume development when the ratio of turbulence integral length scale to the plume width is much larger than unity.

D. Mixing rate

In Sec. III D 1, the mixing rate ω_m for the IECM model valid at small times is obtained using the laminar wake modeling approach. At large times, the mixing rate is taken to be the standard model [Eq. (17)]. Such a specification for the IECM model is compared to the mixing rate used by Sawford.[23] Section III D 2 derives the mixing rate for the modified IECM mixing model along lines similar to Sec. III D 1, imposing conditions of realizability and boundedness.

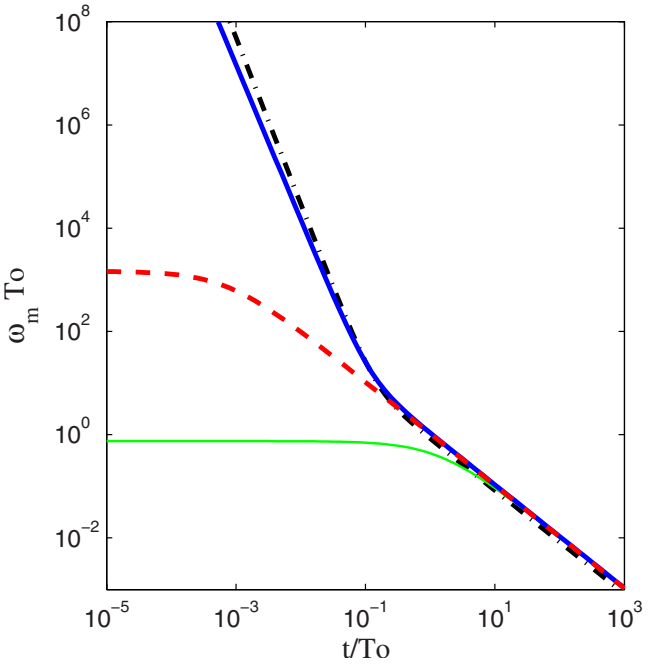

FIG. 3. (Color online) Comparison of mixing rate definitions with flight time from the source: Modified mixing model $\omega_m T_o$ (dashed line); IECM model $\omega_m T_o$ (thick solid line), $\omega_m^{\infty} T_o$ (thin solid line); Sawford's (Ref. 23) empirical mixing rate (dot-dashed line).

1. IECM model

By definition, the IECM model [Eq. (1)] acts to reduce the fluctuations of the scalar about its conditional mean at a rate given by the mixing rate ω_m (which is the inverse of the mixing time scale). The model has no effect on the scalar mean. Molecular diffusion on the other hand has a direct effect on the scalar mean.

With C_ϕ [in Eq. (17)] defined to be a constant, the mixing time scale is proportional to the turbulence time scale for all times during all stages of the plume development. As a consequence, the IECM model (with constant C_ϕ) does not predict the correct evolution of the scalar variance due to the spurious production term in the scalar variance transport equation.

In order to match the laboratory measurements, Sawford[23] used experimental data to obtain an empirically fit time scale of the form

$$\frac{t_m}{t_o} = (\omega_m t_o)^{-1} = 0.6 \frac{t}{t_o}\left[1 + \tanh\left(\frac{\ln(t/t_o) + 2.3}{0.9} \right) \right]. \tag{44}$$

We now develop an alternative specification of the mixing rate which is based on an analytic expression for ω_m at small times, obtained from the laminar thermal wake model. Close to the source, the transport equation for the mean square of scalar [Eq. (31)] can be integrated over y to give the transport equation for the integral mean square of the scalar as

$$\int_{-\infty}^{\infty} \frac{\partial \langle \phi^2 \rangle}{\partial t} dy = -2\omega_m \int_{-\infty}^{\infty} \langle \phi^2 \rangle dy + 2\omega_m \int_{-\infty}^{\infty} \int_{-\infty}^{\infty} \langle \phi | V, y \rangle^2 f_v(V) dV dy. \quad (45)$$

At early times, various moments of the scalar can be obtained from Eq. (42) using the laminar thermal wake modeling approach described in Sec. III C and hence the mixing rate close to the source ω_m^0 is obtained as

$$(\omega_m^0)^{-1} = 2\frac{\bar{\sigma}^3}{\kappa}\left[\frac{1}{\bar{\sigma}} - \frac{1}{\sqrt{\sigma_o^2 + \sigma_y^2(1-\rho_{vy}^2)}}\right]. \quad (46)$$

Let T denote the turbulence time scale $T=k/\varepsilon$ and L the length scale $L=k^{3/2}/\varepsilon$. At the source location, $T_o \equiv T$ $(t=0)$ is simply related to the flight time to the source, t_o as $T_o = t_o/m$. The integral length scale at the source, L_o, can be obtained as $k_o^{3/2}/\varepsilon_o$ where k_o and ε_o refer to the turbulent kinetic energy and dissipation at the source location, respectively. For $t/T_o \ll 1$, Eq. (46) can be simplified to

$$\omega_m^0(t)T_o \approx \frac{m\kappa}{2\sigma_{v_o}^2 T_o}\left(\frac{T_o}{t}\right)^3. \quad (47)$$

The above analysis deduces the appropriate mixing rate $\omega_m^0(t)$ at very early times, whereas the appropriate rate $\omega_m^\infty(t)$ at late times is taken from the standard model [Eq. (17)]. Thus, for $t/T_o \gg 1$ we obtain

$$\omega_m^\infty(t)T_o = \frac{C_\phi \varepsilon T_o}{2k} = \frac{C_\phi}{2}\left(1 + \frac{t}{mT_o}\right)^{-1} \approx \frac{mC_\phi}{2}\frac{T_o}{t}. \quad (48)$$

The specification for the mixing rate (for all times),

$$\omega_m(t) = \omega_m^0(t) + \omega_m^\infty(t), \quad (49)$$

given in nondimensional form as

$$\omega_m(t)T_o = \frac{m\kappa}{2\sigma_{v_o}^2 T_o}\left(\frac{T_o}{t}\right)^3 + \frac{mC_\phi}{2}\left(\frac{T_o}{t}\right), \quad (50)$$

i.e., the sum of the rates given by Eqs. (47) and (48), is comparable to Eq. (44) both near to and far from the source.

2. Modified IECM model

As was done in Sec. III D 1, an analytic expression for the mixing rate ω_m^0 at small times, $t/T_o \ll 1$, can be obtained by conserving the integral of the modeled scalar variance transport equation [Eq. (40)] using the laminar thermal wake model. This approach yields ω_m^0 to be

$$\omega_m^0 \approx \frac{3\kappa}{2\sigma_o^2}. \quad (51)$$

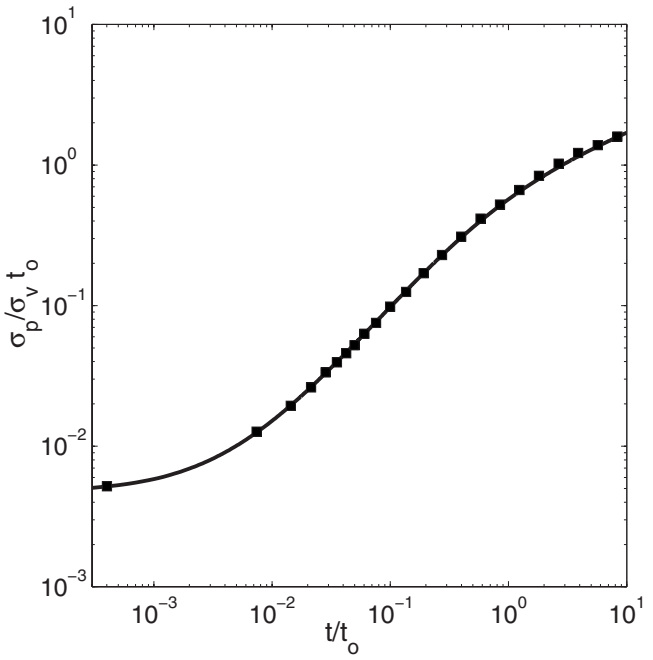

FIG. 4. Width of the mean scalar profile normalized by the turbulence length scale at the source against normalized flight time from the source for source position $x_o/M=52$; σ_p from Eq. (11) (solid line) and σ_p from the present model calculations (■).

However, at large times, $t/T_o \gg 1$, ω_m is taken to be ω_m^∞. Since the two relevant time scales in the passive scalar diffusion from a line source at the source location are the scalar time scale at the source, τ_κ, defined as

$$\tau_\kappa = \frac{\sigma_o^2}{\kappa}, \quad (52)$$

and the turbulence time scale at the source, T_o, their ratio γ can be defined as

$$\gamma \equiv \frac{\tau_\kappa}{T_o}. \quad (53)$$

From Eqs. (48) and (51), the mixing rate that is valid for all times can be specified as

$$\frac{1}{\omega_m(t)} = t_m(t) = \frac{2}{3}\tau_\kappa + [T(t) - T_o]\frac{2}{C_\phi} \quad (54)$$

and in nondimensional form as

$$\frac{1}{\omega_m T_o} = \frac{t_m}{T_o} = \frac{2}{3}\gamma + \left(\frac{T}{T_o} - 1\right)\frac{2}{C_\phi}. \quad (55)$$

In order for the modified IECM mixing model [Eq. (37)] to satisfy realizability and boundedness constraints on the scalar, the mixing rate ω_m should be such that $\omega_m \geq \omega_m^{\min}$ where

$$\omega_m^{\min} = \frac{\kappa}{\tilde{\sigma}^2}, \quad (56)$$

and the specification of the mixing rate [Eq. (55)] satisfies realizability and boundedness for $\gamma < 1$. All the calculations reported are performed with the mixing rate specification

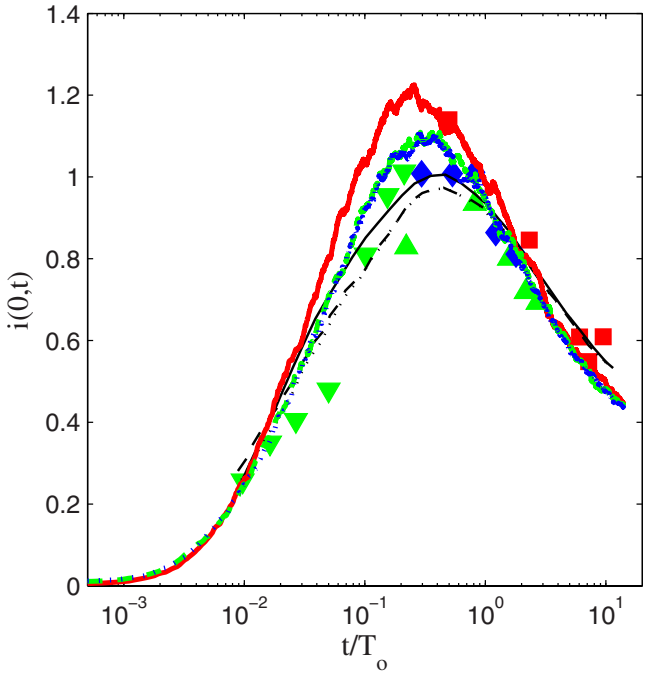

FIG. 5. (Color online) Comparison of the centerline intensity of fluctuations, $i(0,t)$, plotted against flight time from the source. Warhaft (Ref. 7) data: $x_o/M=20$, $\sigma_o=1.27\times10^{-4}$ m (■), $x_o/M=52$, $\sigma_o=2.5\times10^{-5}$ m (▼), $x_o/M=52$, $\sigma_o=1.27\times10^{-4}$ m (▲), and $x_o/M=60$, $\sigma_o=1.27\times10^{-4}$ m (♦). Sawford's (Ref. 23) calculations using the mixing rate given by Eq. (44): $x_o/M=20$, $\sigma_o=1.27\times10^{-4}$ m (thin solid line) and $x_o/M=52$, $\sigma_o=1.27\times10^{-4}$ m (thin dashed line). Present calculations: $x_o/M=20$, $\sigma_o=1.27\times10^{-4}$ m (thick solid line), $x_o/M=52$, $\sigma_o=1.27\times10^{-4}$ m (thick dashed line), and $x_o/M=60$, $\sigma_o=1.27\times10^{-4}$ m (dotted line).

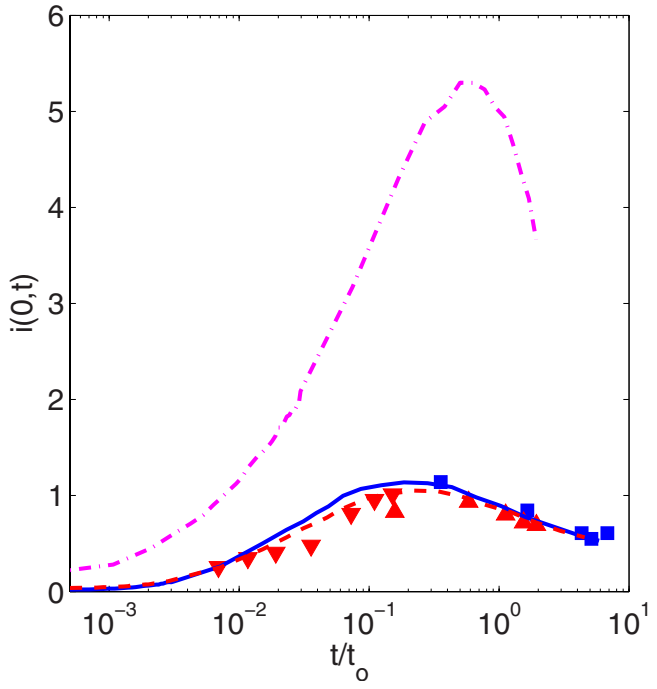

FIG. 6. (Color online) Comparison of IECM model calculations with the mixing rate given by Eq. (17) with the model calculations done with Eq. (50) showing the centerline intensity of fluctuations, $i(0,t)$, against flight time from the source. IECM model calculations using mixing rate given by Eq. (17): $x_o/M=52$, $\sigma_o=1.27\times10^{-4}$ m (thick dot-dashed line). Present calculations: $x_o/M=52$, $\sigma_o=1.27\times10^{-4}$ m (thick dashed line) and $x_o/M=20$, $\sigma_o=1.27\times10^{-4}$ m (thick solid line). Warhaft (Ref. 7) data: $x_o/M=20$, $\sigma_o=1.27\times10^{-4}$ m (■), $x_o/M=52$, $\sigma_o=2.5\times10^{-5}$ m (▼), and $x_o/M=52$, $\sigma_o=1.27\times10^{-4}$ m (▲).

given using Eq. (55). The only adjustable parameter that Eq. (55) is dependent on is the model constant, C_ϕ.

Figure 3 compares the different definitions of the mixing rates given by Eqs. (44), (48), (50), and (55). By construction, the specified mixing rates (50) and (55) smoothly blend into the large-time asymptote (48) and with Eq. (44) for $t/T_o \gg 1$. There is no agreement between Eqs. (44) and (50) for $t/T_o \ll 1$ because Eq. (47) is based on the laminar thermal wake modeling while Eq. (44) is empirically fit to match the wind tunnel laboratory data. Also, Eq. (55) is derived for an entirely different mixing model.

E. Summary of the model

In summary, the modified IECM mixing model, which is used to obtain the results presented in the following sections, consists of Eqs. (9), (10), (37), and (54) [or equivalently Eq. (55) given in nondimensional form]. Unless otherwise stated, the model coefficients take the values $C_0=2.1$ and $C_\phi=1.5$.

IV. IMPLEMENTATION

We represent the flow by an ensemble of $N=10\,000$ particles, which at time t have properties $y(t)$, $v(t)$, and $\phi(t)$. Initially, the solution domain extends between $\pm\Delta_y(0)$, where $\Delta_y(0)=10\sigma_o$. The particles are uniformly distributed in the solution domain and are initialized with a Gaussian

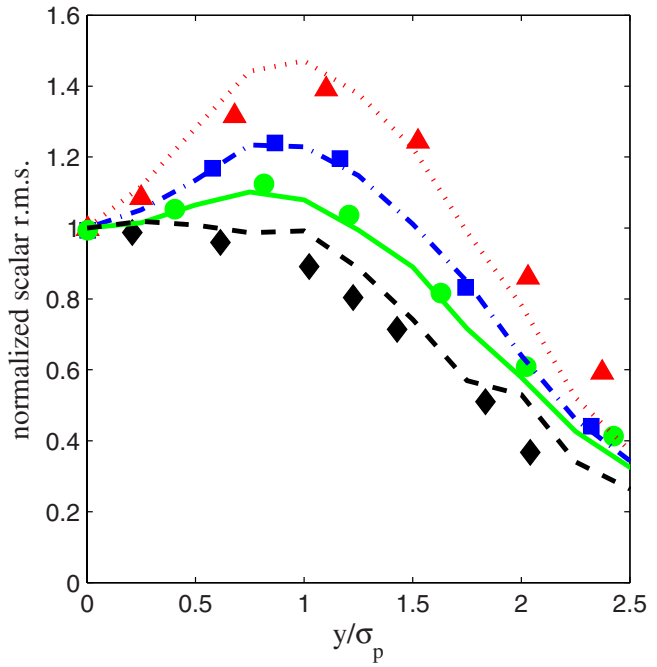

FIG. 7. (Color online) Radial profiles of rms scalar normalized by its centerline value at $x_o/M=52$. Warhaft (Ref. 7) data: $t/t_o=0.007$ (▲), $t/t_o=0.012$ (■), $t/t_o=0.019$ (●), and $t/t_o=1.93$ (♦). Present calculations: $t/t_o=0.007$ (dotted line), $t/t_o=0.012$ (dot-dashed line), $t/t_o=0.019$ (solid line), and $t/t_o=1.93$ (dashed line).

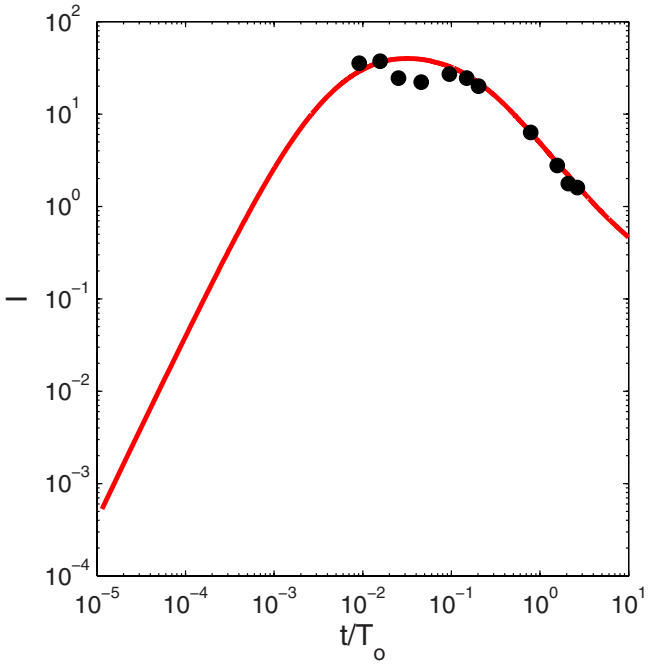

FIG. 8. (Color online) Integral measure of the scalar variance I in nondimensional form against flight time from the source. Present calculations (solid line); Warhaft (Ref. 7) data (●). The source of size $\sigma_o=1.27\times10^{-4}$ m is at $x_o/M=52$.

velocity distribution $\mathcal{N}[0,\sigma_v^2(0)]$. The particles' scalar values are initialized to the mean scalar field (which is a Gaussian with characteristic width σ_o).

The particle properties are advanced in time by a first-order explicit Euler scheme with variable time stepping, the time step Δt being defined as 1/1000 of the mixing time scale, $t_m=1/\omega_m$, where ω_m is given by Eq. (54). For the line source, the modified IECM mixing model (37) reduces to

$$\frac{d\phi}{dt}=\kappa\frac{\partial^2 c}{\partial y^2}-\omega_m(\phi-c), \tag{57}$$

where c is the conditional scalar mean and is known analytically [Eq. (24)]. If the conditional scalar mean is approximated as being a constant across the time step, then, given $\phi(t)$, $\phi(t+\Delta t)$ is known analytically as the solution to Eq. (57),

$$\phi(t+\Delta t)=\phi(t)\exp(-\omega_m\Delta t)+\Pi(t)[1-\exp(-\omega_m\Delta t)], \tag{58}$$

where

$$\Pi(t)=c\left\{\frac{\kappa}{\tilde{\sigma}^2(t)\omega_m}\left[\left(\frac{y(t)-\tilde{y}(t)}{\tilde{\sigma}(t)}\right)^2-1\right]+1\right\} \tag{59}$$

and $\tilde{y}$ and $\tilde{\sigma}$ are given by Eqs. (25) and (26), respectively. The particle's scalar can therefore be advanced in time.

The width of the thermal wake is determined from Eqs. (11) and (12) at the beginning of every time step. When the width of the thermal wake, σ_p, exceeds a quarter of the current domain half-width, $\Delta_y(t)$, the solution domain is expanded as follows. The size of the solution domain is doubled. An additional N particles are temporarily introduced into the expanded domain such that the resulting particle distribution is uniform in physical space. Since the computational cost scales linearly with the number of particles for a given time step, to keep the computational cost constant, only every alternate particle of the $2N$ particles is retained in the newly expanded domain. In additional to cost control, this procedure also ensures that the thermal wake is well resolved within the solution domain. For the time period of the simulation, there are a significant number of particles per unit turbulence integral scale, and hence only the resolution of the thermal wake is of concern. Reflective boundary conditions are applied at the domain boundaries.

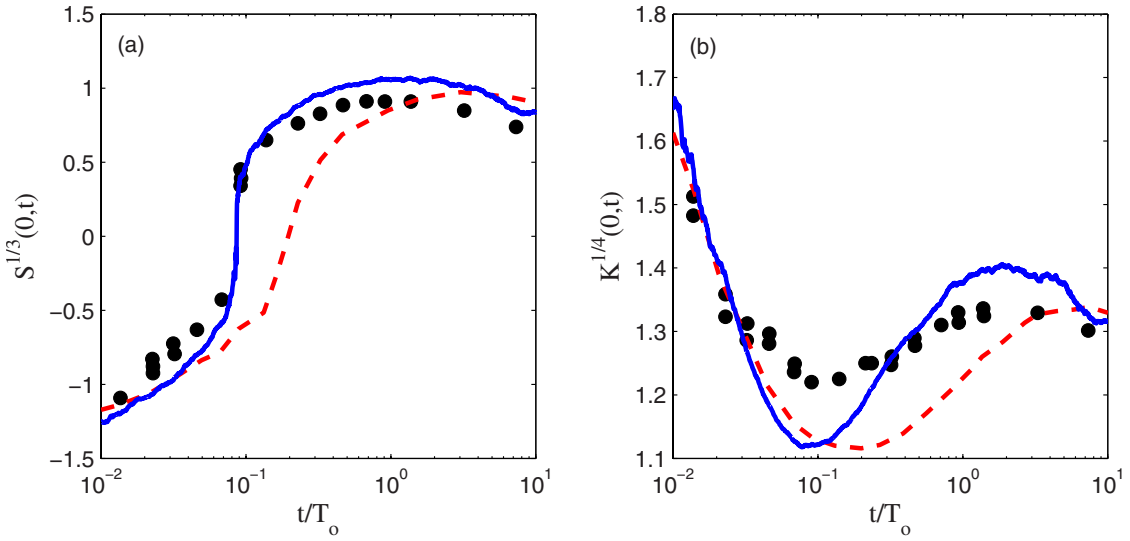

FIG. 9. (Color online) Higher moments on the centerline against flight time from the source: Present calculations (solid line); Sawford (Ref. 23) IECM calculations (dashed line); Sawford and Tivendale (Ref. 23) data (●): (a) skewness S and (b) kurtosis K.

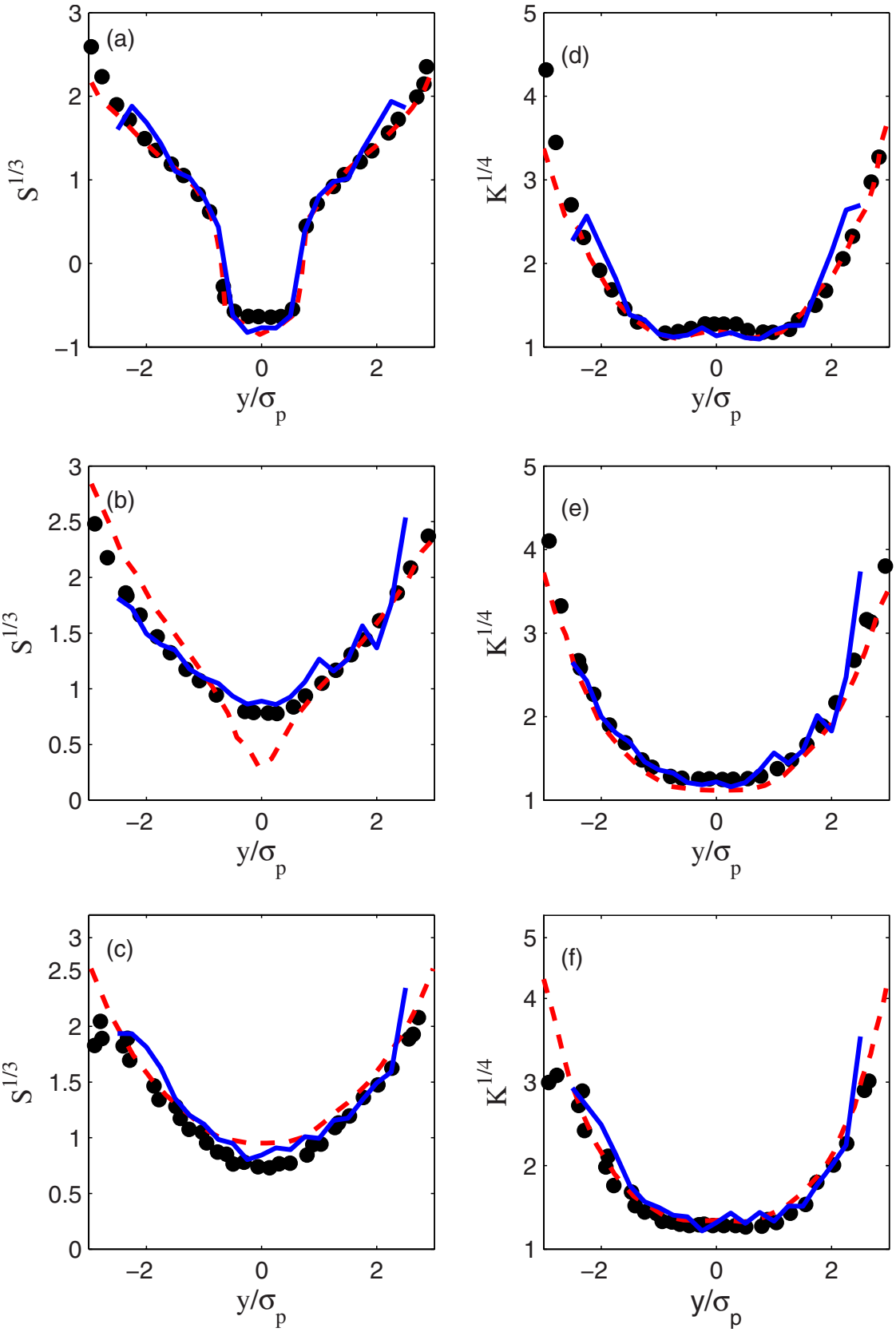

FIG. 10. (Color online) Radial profiles of higher-order moments measured at varying distances from the source. Present calculations (solid line); Sawford (Ref. 23) IECM calculations (dashed line); Sawford and Tivendale (Ref. 23) data (●): (a) skewness at t/T_o=0.0014, (b) skewness at t/T_o=0.22, (c) skewness at t/T_o=7.2, (d) kurtosis at t/T_o=0.0014, (e) kurtosis at t/T_o=0.22, and (f) kurtosis at t/T_o=7.2.

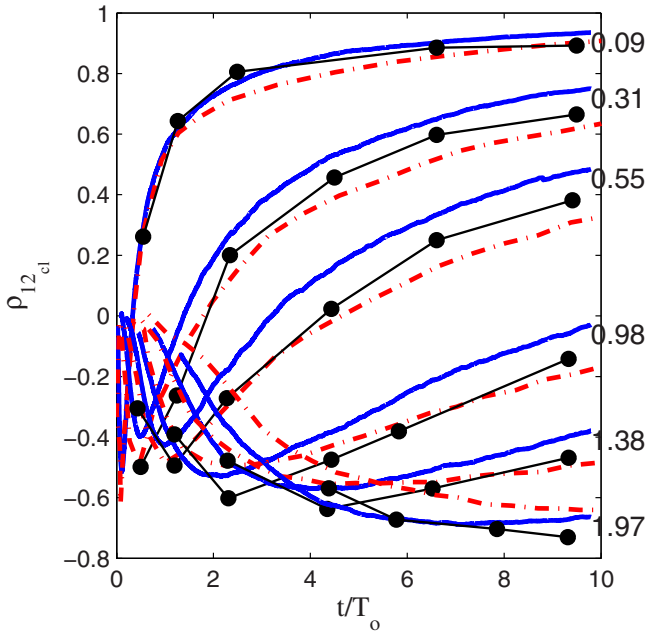

FIG. 11. (Color online) Evolution of the centerline cross-correlation coefficient for various source spacings, $d_o/M=0.09,0.31,0.55,0.98,1.38,1.97$. The sources are placed at a distance of $x_o/M=20$ from the turbulence generating grid: Warhaft (Ref. 7) data (●); Sawford (Ref. 23) model calculations (dot-dashed line); present calculations (solid line).

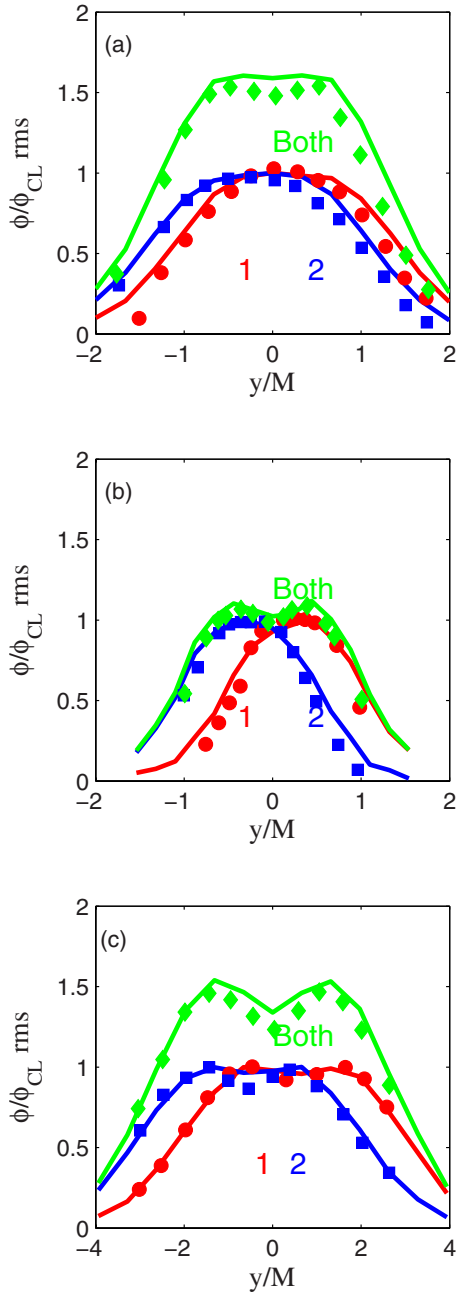

FIG. 12. (Color online) Radial profiles of rms scalar normalized by their respective centerline values when the sources are positioned at $x_o/M=20$ from the turbulence grid for different spacings between the sources, d_o: (a) $d_o/M=0.31$ and $t/T_o=2.31$, (b) $d_o/M=0.55$ and $t/T_o=1.19$, and (c) $d_o/M=0.98$ and $t/T_o=9.31$; present model calculations (solid line); Warhaft (Ref. 7) data: ϕ_1 (●), ϕ_2 (■), and $\phi_1+\phi_2$ (◆).

Figure 4 plots the normalized width of the mean scalar profile (obtained using a quantile-quantile plot of particle position compared to an error function) against normalized flight time from the source. The good agreement between the theoretical prediction[22] given by Eqs. (11) and (12) and model calculations using the modified IECM model verifies the numerics of the calculations—at least for the scalar mean.

The radial profiles of various statistics used to compare the present model calculations with the experimental data are obtained by binning the particles in physical space, in bins of size approximately half of σ_p. Small bins give rise to larger statistical errors while large bins smear out the gradients. This smearing probably explains the small discrepancies between the model calculations and experimental data in regions with steeper gradients (shown in the later sections). Various statistics are obtained by averaging over 20 independent simulations.

V. RESULTS AND DISCUSSION

A. A single line source

Detailed PDF calculations have been performed with the modified IECM model using the mixing rate given by Eq. (55), and the results are compared to the experimental data of Warhaft[7] and the previous calculations of Sawford.[23] Higher-order scalar moments, namely, skewness and kurtosis, are also compared against the experimental data of Sawford and Tivendale reported by Sawford.[23]

Figure 5 plots the centerline intensity of fluctuations, $i(0,t)=\langle\phi'^2\rangle_{y=0}^{1/2}/\langle\phi\rangle_{y=0}$, against flight time from the source for various source conditions as detailed in the figure. The experiments are performed with two source sizes. The larger source is used when measurements are taken at distances far away from the source for $x_o/M=20$ so that the measurements are not corrupted by background noise. Since the model calculations are oblivious to such effects, only one source size is used. The centerline intensity of fluctuations agrees well with the experimental data and with the previous model calculations of Sawford[23] throughout the development of the plume. Contrasting this against Fig. 6 in which the IECM model with Eq. (17) is used and molecular diffusion is neglected in the scalar evolution equation, we see that molecu-

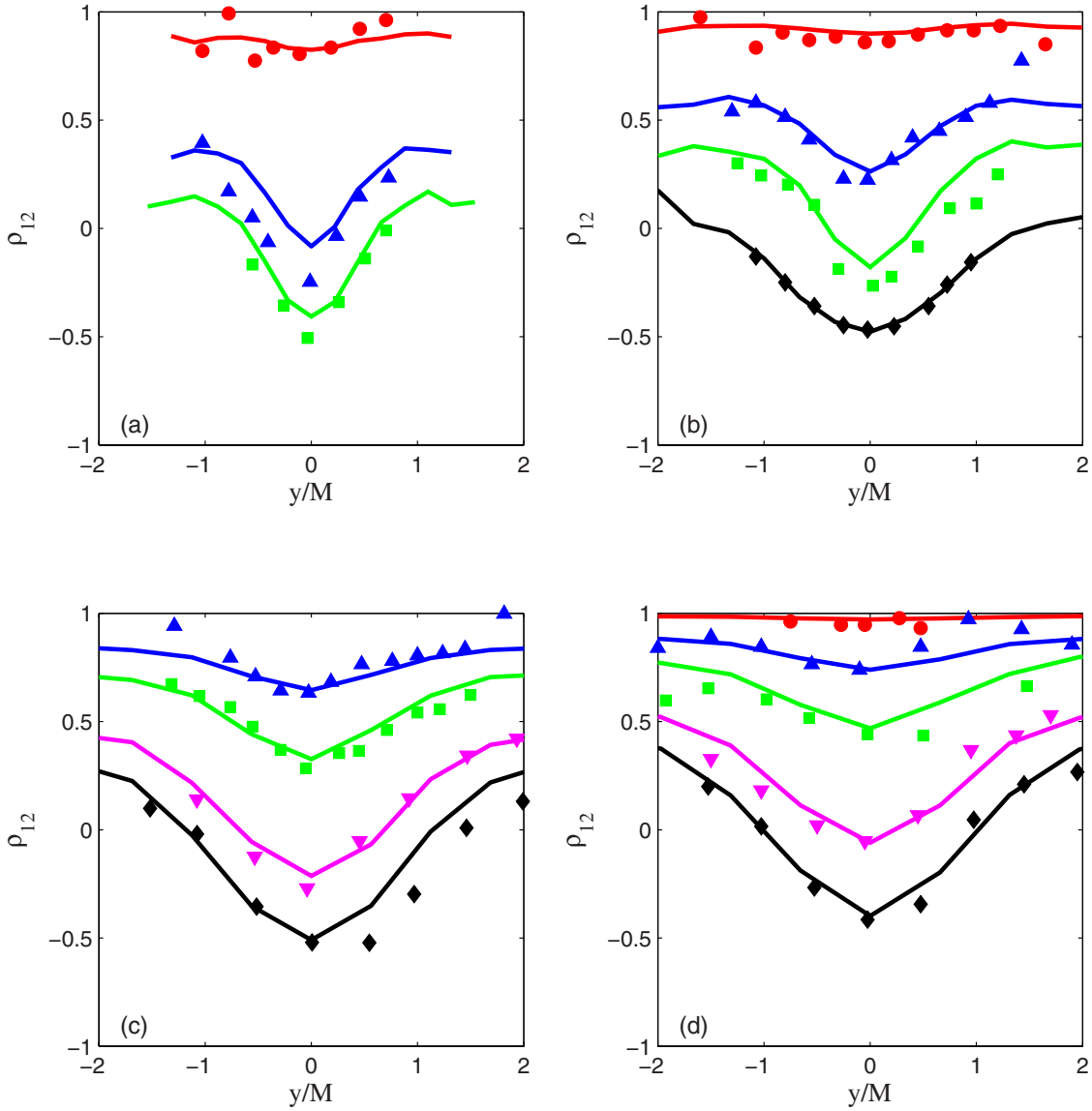

FIG. 13. (Color online) Radial profiles of the cross-correlation coefficient ρ_{12} between sources 1 and 2 for different spacings between the two sources, d_o/M. The sources are positioned at $x_o/M=20$ from the turbulence generating grid: (a) $t/T_o=1.19$, (b) $t/T_o=2.31$, (c) $t/T_o=6.51$, and (d) $t/T_o=9.31$. Present model calculations (solid line). Warhaft (Ref. 7) data: $d_o/M=0.05$ (●), $d_o/M=0.31$ (▲), $d_o/M=0.55$ (■), $d_o/M=0.98$ (▼), and $d_o/M=1.38$ (♦).

lar diffusion effects are significant in the correct estimation of the evolution of the scalar variance in both near-field and far-field stages of the plume development.

Radial profiles of the normalized rms scalar at four distinct stages of the plume development are plotted in Fig. 7 and the integral measure of the variance, $I=\int\langle\phi'^2\rangle dy$ normalized by $2\pi L_o/Q^2$ is plotted in Fig. 8. The present calculations are successful in predicting both the shape of the profiles and also the locations of the extrema at various time instants in the development of the thermal wake and there is good agreement with the experimental data.

It is also of significant interest to study the model predictions of the higher-order scalar moments especially skewness and kurtosis. Experimental data from Sawford and Tivendale reported by Sawford[23] and previous IECM model calculations from Sawford[23] are used to compare with the model predictions. Figure 9 plots the centerline values of skewness S and kurtosis K against flight time from the source while Fig. 10 compares the radial profiles of the skewness and kurtosis measurements made at three different times, $t/T_o=0.0014, 0.22, 7.2$, with the experimental data. Even though the centerline values of the moments are not in perfect agreement with the data for all times, the radial profiles match the experimental observations well. However, the centerline predictions are more accurate than the previous model calculations.

B. A pair of line sources

A nontrivial extension can be made from a single line source to a pair of line sources in grid turbulence. The two sources, numbered 1 and 2, are placed parallel to each other separated by a distance d_o at a distance x_o from the turbulence generating grid. The origin of the coordinate system is chosen so that the locations of the sources are $(x,y)=(x_o,\pm d_o/2)$. In the experiments, a range of source separa-

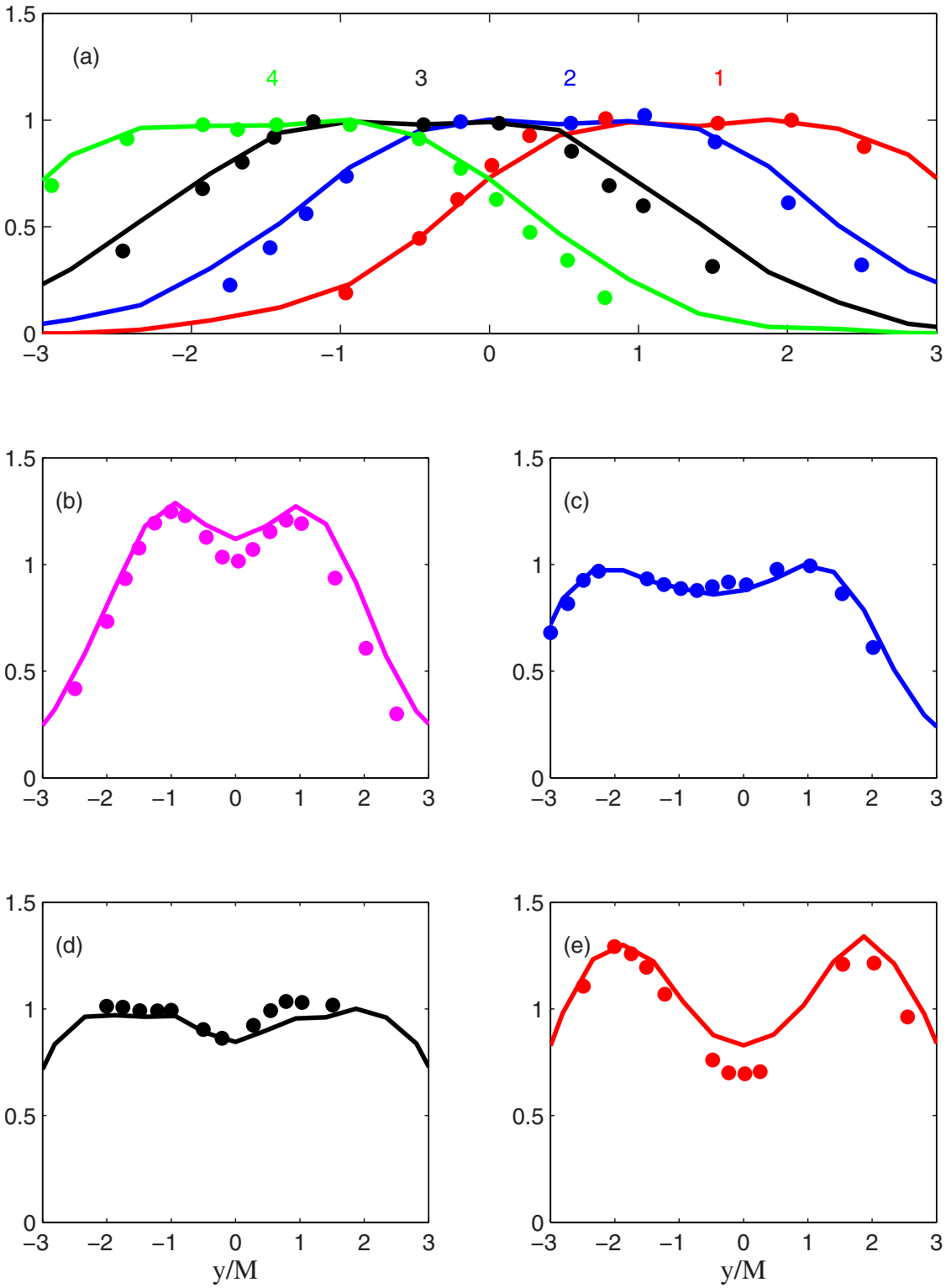

FIG. 14. (Color online) (a) Radial profiles of rms scalar corresponding to each of the four sources in an array, normalized by their respective centerline values at $t/T_o=4.41$; (b) radial profiles of rms scalar corresponding to $\phi_2+\phi_3$; (c) radial profiles of rms scalar corresponding to $\phi_2+\phi_4$; (d) radial profiles of rms scalar corresponding to $\phi_1+\phi_4$; (e) radial profiles of rms scalar corresponding to all the four sources. The radial profiles in (b)–(e) are normalized by the mean centerline value obtained from (a). Present model calculations (solid line); Warhaft (Ref. 7) data (●).

tions was considered, from $d_o=1.2$ mm to $d_o=127$ mm. We are interested in modeling the mixing and interference of the plumes from these two line sources.

The scalar fields corresponding to the two sources 1 and 2 are denoted in the laboratory frame by $\phi_1(x,y)$ and $\phi_2(x,y)$, respectively. The means and variances of ϕ_1 and ϕ_2 are the same as for the single source (with the appropriate shift in origin). In the moving reference frame, the scalar fields are denoted by $\phi_1(y,t)$ and $\phi_2(y,t)$. The correlation coefficient, $\rho_{12}(y,t)$, is defined as

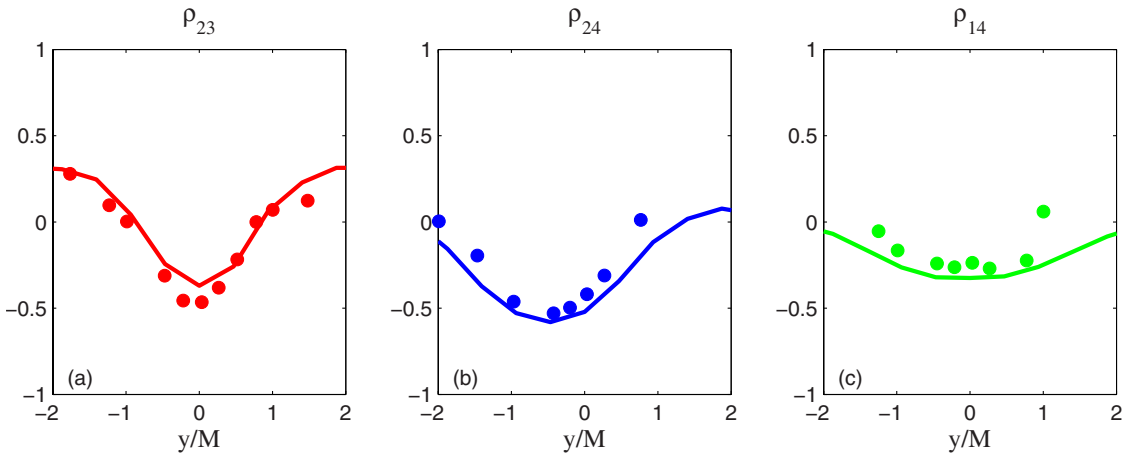

FIG. 15. (Color online) Radial profiles of the cross-correlation coefficient ρ between pairs of sources at $t/T_o=4.41$. Diffusion behind an array of four sources is considered. The sources are positioned at $x_o/M=20$ from the turbulence grid: (a) $d_o/M=1$, sources 2 and 3; (b) $d_o/M=2$, sources 2 and 4; (c) $d_o/M=3$, sources 1 and 4. Present model calculations (solid line); Warhaft (Ref. 7) data (●).

$$\rho_{12}=\frac{\langle\phi_1'\phi_2'\rangle}{\langle\phi_1'^2\rangle^{1/2}\langle\phi_2'^2\rangle^{1/2}}, \tag{60}$$

where $\phi_j'=\phi_j-\langle\phi_j\rangle$ is the fluctuation in the jth scalar about its mean.

In the present work, the PDF model using Eq. (55) is applied to a pair of line sources and is used to calculate the correlation coefficient ρ_{12}. Each particle in the simulation now has two properties, ϕ_1 and ϕ_2, in addition to its velocity and position. Each $\phi_j, j=1,2$, evolves by the modified IECM model Eq. (37) with conditional means defined similarly to Eq. (24) relative to their respective sources. For instance, the conditional mean, $\langle\phi_1|y,v\rangle$, is given by

$$\langle\phi_1|y,v\rangle=\frac{Q}{\sqrt{2\pi}\sqrt{\sigma_o^2+\sigma_y^2(1-\rho_{vy}^2)}}\times\exp\left[-\frac{1}{2}\left(\frac{y-d_o/2-\rho_{vy}v\sigma_y/\sigma_v}{\sqrt{\sigma_o^2+\sigma_y^2(1-\rho_{vy}^2)}}\right)^2\right], \tag{61}$$

where source 1 is located at a distance $d_o/2$ from the origin. Thus, the correlation coefficient can be calculated and compared to the detailed laboratory measurements available.[7] The experimental data for the pair of line sources form part of the same data set as the single line source. The relevant parameters are listed in Table I with $\sigma_o=1.27\times10^{-4}$ m and $x_o/M=20$.

In the experiments, the correlation coefficient can be estimated with multiple sources that are sometimes on or off using the inference method.[8] For a pair of line sources, let ϕ_B correspond to the scalar field when both the sources are active. Then, with the assumption that the two scalar fields are linearly additive, we can write

$$\phi_B=\phi_1+\phi_2, \tag{62}$$

$$\phi_B'=\phi_1'+\phi_2', \tag{63}$$

$$\langle\phi_B'^2\rangle=\langle\phi_1'^2\rangle+\langle\phi_2'^2\rangle+2\langle\phi_1'\phi_2'\rangle. \tag{64}$$

Therefore, using Eqs. (60) and (64) the correlation coefficient can be written as

$$\rho_{12}=\frac{\langle\phi_B'^2\rangle-\langle\phi_1'^2\rangle-\langle\phi_2'^2\rangle}{2\langle\phi_1'^2\rangle^{1/2}\langle\phi_2'^2\rangle^{1/2}}. \tag{65}$$

(This technique is used in the experiments, whereas in the calculations, joint statistics of the scalars are extracted from the particles' scalar values.)

The evolution of the centerline correlation coefficient between the two sources is plotted in Fig. 11 for a range of source separations. The present model calculations are compared to the previous calculations of Sawford[23] and laboratory data of Warhaft.[7] The present model calculations correctly predict the evolution of the centerline correlation coefficient for a range of source separations.

The scalar rms is a relative quantity dependent on the strength of the source. In order to make comparisons with laboratory data, the scalar rms profiles are normalized by the centerline scalar rms for a single source. Figure 12 compares the model predictions of the normalized radial profiles of rms scalar with experimental data for three different source spacings, $d_o(mm)=8,14,25$. The plots show the rms scalar profiles for ϕ_1, ϕ_2, and $\phi_1+\phi_2$ assuming that the scalar fields

TABLE III. Parameters in the laboratory measurements of Warhaft and Lumley (Ref. 6). Definitions are given in Table I.

σ_o	3.21×10^{-4}	m
M	2.54×10^{-2}	m
x_o/M	20	
U	6.5	ms^{-1}
$\sigma_u,\sigma_v,\sigma_w$	2.275	ms^{-1}
m	1.34	
κ	2.26×10^{-5}	$m^2\ s^{-1}$

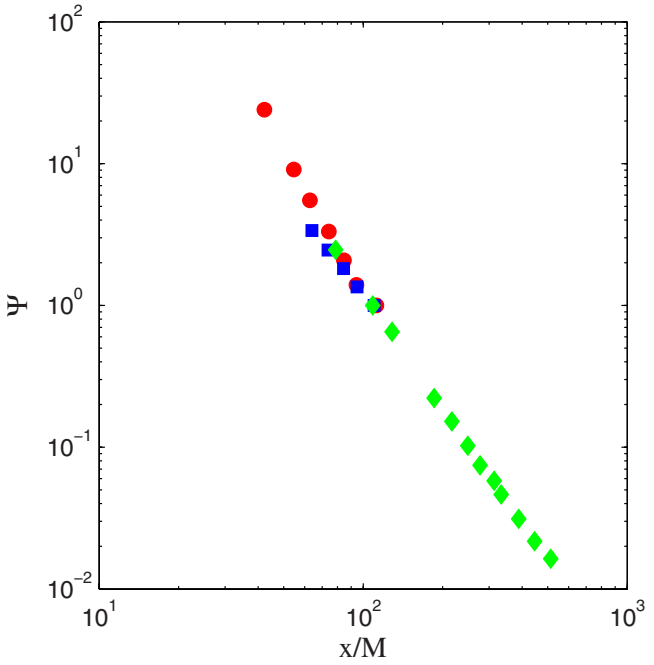

FIG. 16. (Color online) Experimental data of decay of normalized scalar fluctuations, $\Psi=\langle\phi'^2\rangle/\langle\phi'^2\rangle_{x/M=100}$, downstream of a heated mandoline from the turbulence generating grid. Relevant parameters are listed in Table III: $d_o/M=1$ and $x_o/M=20$ (●), $d_o/M=2$ and $x_o/M=20$ (■), and $d_o/M=2/3$ and $x_o/M=44$ (♦).

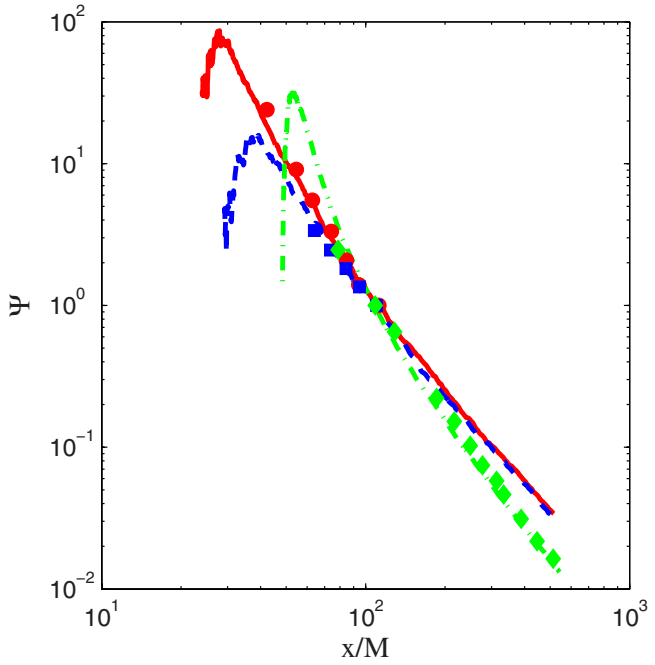

FIG. 17. (Color online) Decay of normalized scalar fluctuations, $\Psi=\langle\phi'^2\rangle/\langle\phi'^2\rangle_{x/M=100}$, downstream of a heated mandoline from the turbulence generating grid. Experimental data: $d_o/M=1$ and $x_o/M=20$ (●), $d_o/M=2$ and $x_o/M=20$ (■), and $d_o/M=2/3$ and $x_o/M=44$ (♦). Present model calculations are denoted by lines: $d_o/M=1$ and $x_o/M=20$ (solid line), $d_o/M=2$ and $x_o/M=20$ (dashed line), and $d_o/M=2/3$ and $x_o/M=44$ (dot-dashed line).

are linearly additive. The present model calculations, as can be seen, correctly reproduce the laboratory measurements.

The radial profiles of the correlation coefficient ρ_{12} can be obtained using Eq. (60) in the model calculations and are plotted in Fig. 13 at different stages in the plume development. At every stage, multiple source separations are considered and comparison is made with the experimental data. The agreement is good as regards both the shape of the profile and the location of the minima on the centerline between the two sources. [The overprediction in ρ_{12} seen at $y/M=0$ in Fig. 13(a) may be due to the smearing introduced by the binning used to extract statistics.]

C. An array of line sources

The decay of the scalar variance downstream of a heated mandoline (a set of multiple line sources placed parallel to one another a distance x_o downstream of the turbulence generating grid) can be understood by studying the interference between multiple line sources.[7]

As the first step, an array of four line sources is considered in place of the pair of sources in Sec. V B. The relevant parameters for diffusion behind an array of four line sources are listed in Table I with $\sigma_o=1.27\times10^{-4}$ m and $x_o/M=20$. The distance between adjacent line sources is d_o and will be referred to as the mandoline spacing later on in the section.

As in Sec. V B, PDF calculations are performed with the modified IECM model by making a simple extension to four line sources. The sources are located at a distance of $x_o/M=20$ from the turbulence grid and adjacent sources are separated by a nondimensional distance of $d_o/M=1$. The mea-

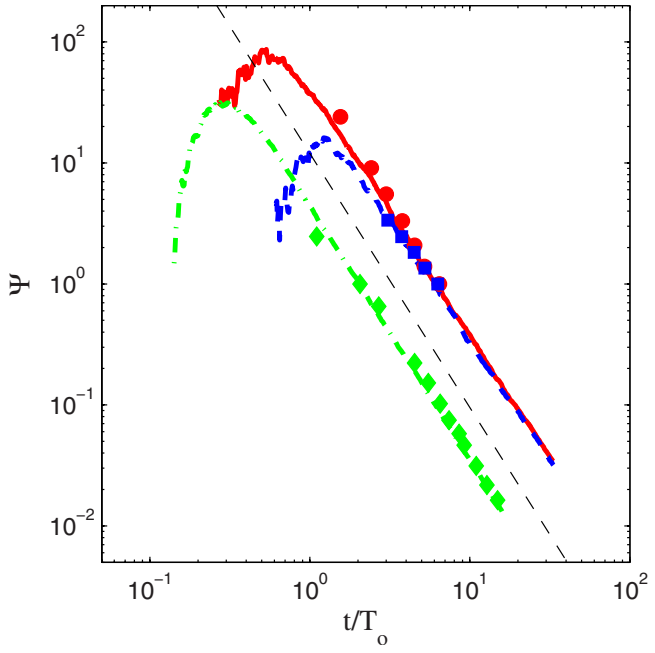

FIG. 18. (Color online) Decay of normalized scalar fluctuations, $\Psi=\langle\phi'^2\rangle/\langle\phi'^2\rangle_{x/M=100}$, against flight time from the source. Experimental data: $d_o/M=1$ and $x_o/M=20$ (●), $d_o/M=2$ and $x_o/M=20$ (■), and $d_o/M=2/3$ and $x_o/M=44$ (♦). Present model calculations are denoted by lines: $d_o/M=1$ and $x_o/M=20$ (solid line), $d_o/M=2$ and $x_o/M=20$ (dashed line), and $d_o/M=2/3$ and $x_o/M=44$ (dot-dashed line). A dashed line of slope $-mC_\phi=-2.1$ is shown for reference.

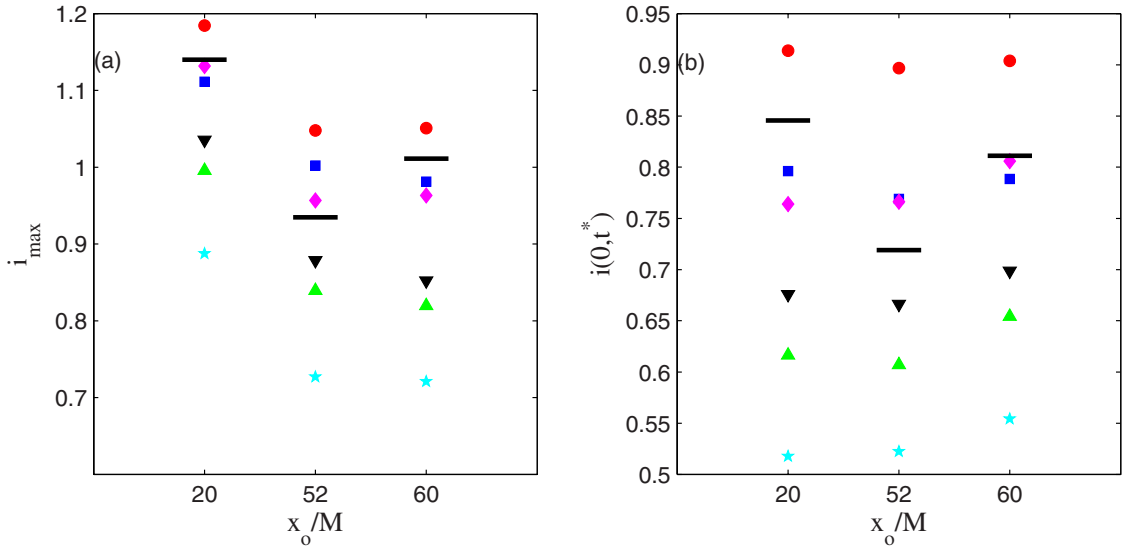

FIG. 19. (Color online) Effect of model coefficients C_0 and C_ϕ on scalar fluctuations. (a) Maximum centerline intensity of fluctuations, $i_{\max}$, against different placements of the source with respect to the turbulence grid, x_o/M. (b) Centerline intensity of fluctuations, $i(0,t^*)$, against x_o/M where $t^*/T_o=1.82$. Symbols are from present calculations for different combinations of C_0 and C_ϕ: $C_0=2.1$ and $C_\phi=1.3$ (●), $C_0=2.1$ and $C_\phi=1.5$ (■), $C_0=2.1$ and $C_\phi=2$ (▲), $C_0=3$ and $C_\phi=1.3$ (♦), $C_0=3$ and $C_\phi=1.5$ (▼), and $C_0=3$ and $C_\phi=2$ (★). Solid horizontal lines correspond to the experimental data.

surements are made at a distance of $x'/M=63$ from the sources or equivalently at a time instant of $t/T_o=4.41$. The origin of the coordinate system is defined at the midpoint between the four line sources i.e., the four sources are located at $(x,y)=[x_o, \pm(2j-1)d_o/2]$, $j=1,2$.

Figure 14 plots the radial profiles of the normalized scalar rms. Normalization is done with respect to the scalar rms value on the centerline of a single source. The radial profiles of the scalar rms corresponding to each source is plotted in (a) for all the four sources numbered 1–4. Each of these profiles is statistically identical to the single line source but shifted in physical space appropriately. Subfigures (b), (c), and (d) plot the radial profiles of scalar rms corresponding to $\phi_j+\phi_k$, $|j-k|=1,2,3$, respectively. The profiles are shifted appropriately in physical space depending on the choice of the sources, j and k. Finally subfigure (e) plots normalized rms scalar profile for $\Sigma_{j=1}^4\phi_j$. The effect of the interference between multiple line sources in reducing the total rms at the centerline between the four sources is captured by the model calculations and the agreement with the experimental data is good.

The radial profiles of the pairwise correlation coefficients for sources separated by distances $d_o/M=1,2,3$ are plotted in Figs. 15(a)–15(c), respectively. Each of the curves here is obtained from the data in Figs. 14(a)–14(d). This confirms that the individual rms profiles and the pairwise correlation coefficients are sufficient to estimate the rms scalar profile corresponding to $\Sigma_{j=1}^4\phi_j$.

D. The heated mandoline

The decay of scalar variance downstream of a heated mandoline is equivalent to considering the interference between multiple line sources equally spaced and placed parallel to each other at some distance from the turbulence generating grid.[7] Over the downstream range of the experiments, the scalar variance in a given experiment appears to decay according to the power law

$$\frac{\langle\phi'^2\rangle}{T^2}=B\left(\frac{x}{M}\right)^{-n}, \quad x>x_o, \tag{66}$$

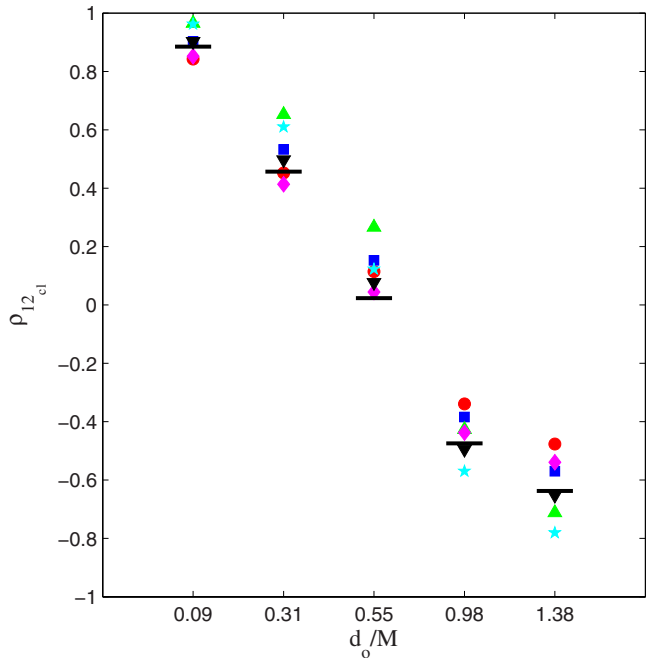

FIG. 20. (Color online) Correlation coefficient between a pair of line sources at $t/T_o=2.8$ plotted for different source separations, $d_o/M=0.09,0.31,0.55,0.98,1.38$, for various combinations of C_0 and C_ϕ. Symbols are from present calculations for different combinations of C_0 and C_ϕ: $C_0=2.1$ and $C_\phi=1.3$ (●), $C_0=2.1$ and $C_\phi=1.5$ (■), $C_0=2.1$ and $C_\phi=2$ (▲), $C_0=3$ and $C_\phi=1.3$ (♦), $C_0=3$ and $C_\phi=1.5$ (▼), and $C_0=3$ and $C_\phi=2$ (★). Solid horizontal lines correspond to the experimental data.

TABLE IV. Parameters corresponding to the cases performed in Sec. V F. Velocity variance at the source location (isotropic turbulence), $\sigma_{v_o}^2$, Velocity variance decay exponent m, turbulence mesh spacing M, mean speed U, source size σ_o, Taylor scale Reynolds number at the source location, R_λ, and ratio of source to turbulence integral scale at the source location, Λ.

	$\sigma_{v_o}^2$ (m^2/s^2)	m	M (cm)	U (m/s)	σ_o (m)	R_λ	Λ
1	0.45	1.2	11.4	3.66	2.5×10^{-5}	400	5.8×10^{-5}
2	0.45	1.2	11.4	3.66	2.01×10^{-3}	400	4.7×10^{-4}
3	2.35	1.2	5	8.35	2.5×10^{-5}	400	1.3×10^{-4}
4	0.36	1.2	5	3.26	2.5×10^{-5}	250	1.3×10^{-4}
5	5.6	1.2	11.4	12.88	5.7×10^{-5}	750	1.3×10^{-4}

where x is measured from a virtual origin (within a few mesh lengths of the grid), T is the mean temperature of the flow without any of the sources being active, n is the scalar variance decay exponent, and B is a constant. From the experiments of Warhaft and Lumley,[6] the scalar variance decay rate was found to be uniquely determined by the length scale of the initial scalar fluctuations relative to the integral turbulence length scale. The scalar variance decay rate n was shown to completely depend on the wavelength of the initial scalar field determined by the mandoline spacing d_o.

The relevant turbulence parameters characterizing the experimental data are listed in Table III. The experiments were carried out with the mandoline placed a distance $x_o/M=20$ and for two configurations of the mandoline with spacings of $d_o/M=1$ and 2. The scalar variance decay exponents were empirically obtained to be $n=3.20$ and 2.06, respectively, for the two mandoline configurations.

In the present calculations, PDF calculations similar to the array of line sources (described in Sec. V C) are performed to compare with the experimental data for the two mandoline configurations. The model calculations are performed with a number of line sources, n_s, such that the addition of any more line sources would hardly affect the scalar variance at the measurement point. Closer to the source (in the laboratory frame of reference), fewer sources are sufficient, while farther away, more are required.

Figure 16 plots the experimental data from Warhaft and Lumley[6] for $d_o/M=1,2$ and Warhaft[7] for $d_o/M=2/3$ of the decay of the scalar variance downstream of the turbulence grid. Figure 17 compares the model calculations against the experimental data and there is clearly a good match between the two. Plotting the scalar variance with distance from the turbulence grid does show a dependence on the ratio of the length scale of the initial scalar fluctuations to the integral turbulence length scale. On the other hand, Fig. 18 plots the same data, both numerical and experimental, as a function of flight time from the source, t/T_o, and the constant decay rate in the scalar fluctuations is apparent across all d_o/M beyond a certain value of t/T_o. For large times, the model predicts a decay exponent of mC_ϕ which evaluates to 2.1 for $C_\phi=1.5$

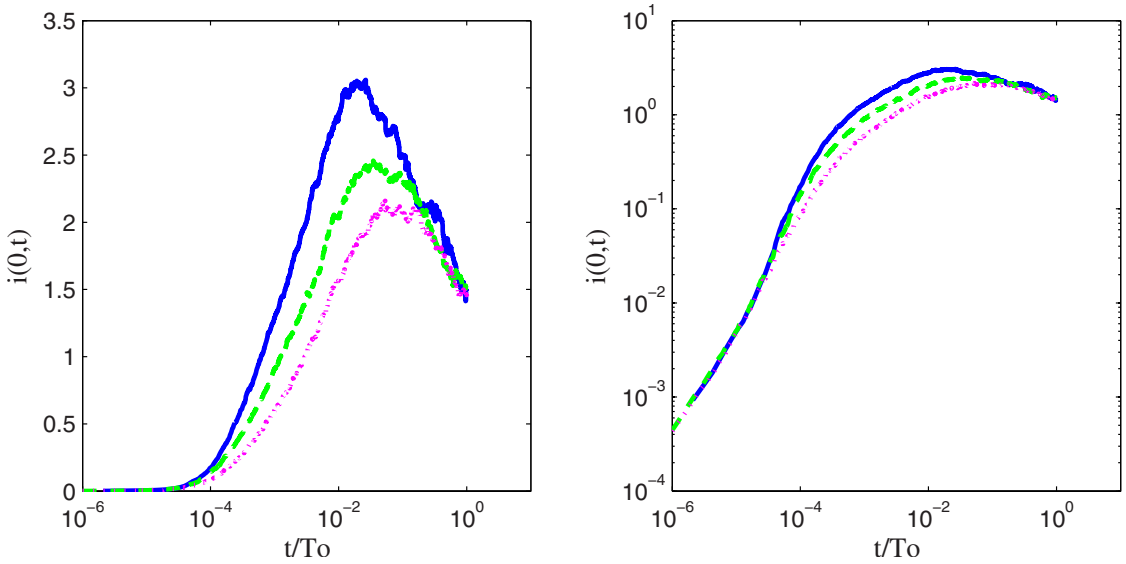

FIG. 21. (Color online) Centerline intensity of fluctuations, $i(0,t)$, vs flight time from the source for $\Lambda=1.3\times10^{-4}$ and different values of R_λ: $R_\lambda=750$ (solid line), $R_\lambda=400$ (dashed line), and $R_\lambda=250$ (dotted line).

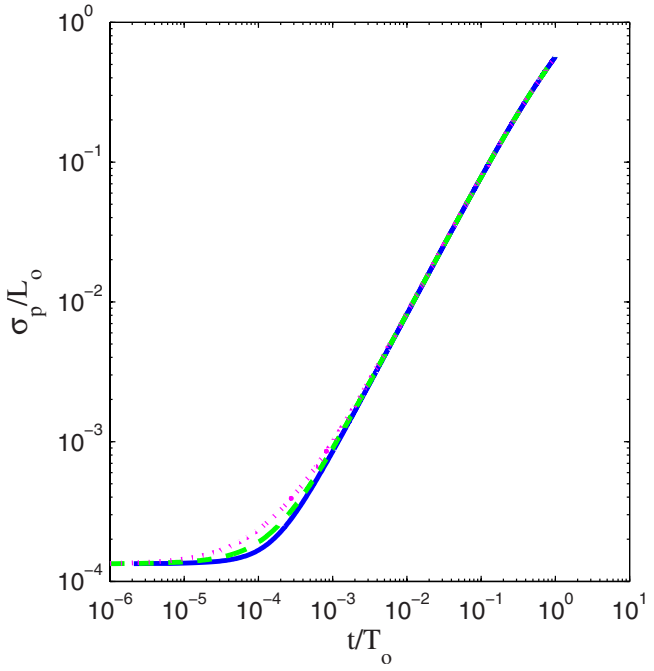

FIG. 22. (Color online) Mean plume width normalized by the turbulence integral scale at the source, L_o, against flight time from the source for $\Lambda = 1.3 \times 10^{-4}$ and different values of R_λ: $R_\lambda = 750$ (solid line), $R_\lambda = 400$ (dashed line), and $R_\lambda = 250$ (dotted line).

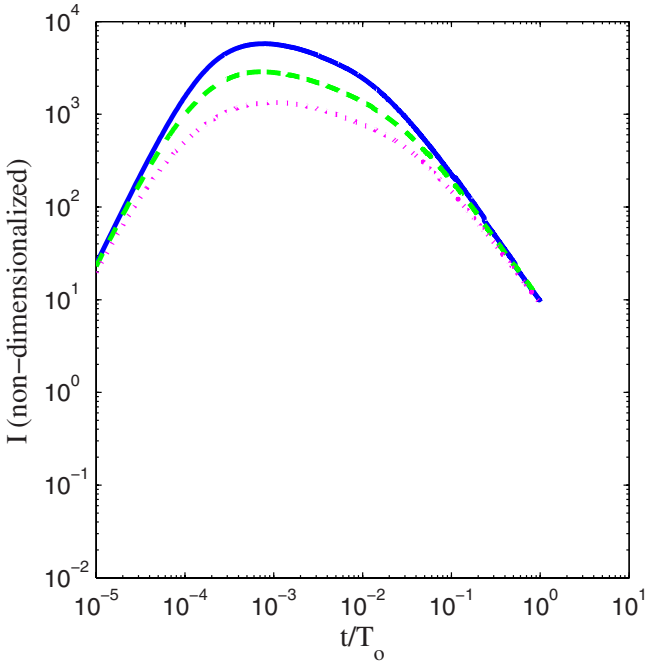

FIG. 23. (Color online) Integral of scalar variance, I, normalized by $2\pi L_o/Q^2$ against flight time from the source for $\Lambda = 1.3 \times 10^{-4}$ and different values of R_λ: $R_\lambda = 750$ (solid line), $R_\lambda = 400$ (dashed line), and $R_\lambda = 250$ (dotted line).

and both the calculations and experimental data agree with the model prediction. This is consistent with the findings of Sreenivasan *et al.*[29] who observed from their heated mandoline experiments that the scalar variance decays at a constant rate independent of x_o and d_o/M. The measured decay exponent from their experiments is 2.2 (i.e., within 5% of that from the present model).

E. The effect of the choices of C_0 and C_ϕ

All results reported so far were performed using the standard values of $C_0 = 2.1$ and $C_\phi = 1.5$, whereas the calculations of Sawford[23] for both the single and pair of line sources are presented for $C_0 = 3$. In order to study the effect of the choice of the above mentioned model parameters, calculations were repeated for the different combinations of $C_0 = 2.1$, 3 and $C_\phi = 1.3$, 1.5, 2 and compared to the experimental data.

Figure 19 compares the centerline intensity of fluctuations, $i(0,t)$, for the six different combinations of C_0 and C_ϕ with the experimental data for three placements of the source, $x_o/M = 20, 52, 60$. Subplot (a) compares the maximum of i observed from the experiments for a given x_o/M to the estimates obtained from the present calculations at the same time. Subplot (b) compares the experimentally observed value of $i(0,t^*)$, where $t^*/T_o \sim 1.82$ to the calculations at the same time. The value $C_\phi = 2$ underpredicts the scalar variance irrespective of C_0, whereas $C_\phi = 1.3$ yields better agreement with the experimental data. Our choices of $C_0 = 2.1$ and $C_\phi = 1.5$ compare well with the $C_0 = 2.1$ and $C_\phi = 1.3$ combination at least for the single line source.

Similarly, Fig. 20 compares the estimated centerline correlation coefficient $\rho_{12_{cl}}$ between a pair of line sources using different combinations of model parameters to the experimentally observed value at the same time for various source separations at a time instant of $t/T_o \sim 2.8$. The combination of $C_0 = 3$ and $C_\phi = 1.5$ yields the most accurate results but, as for the single line source, our choice of the model parameters gives results with a reasonable accuracy.

F. Effect of the Reynolds number and source size

Presently, the experimental data available for dispersion studies behind line sources in decaying grid turbulence are at relatively small Taylor scale Reynolds numbers, $R_\lambda \sim 60$. As a natural consequence, it is of significant relevance to be able to understand and predict the behavior of the scalar field at higher Reynolds numbers.

From the experimentalists' viewpoint, for a grid of fixed geometry, the problem of dispersion from a single line source requires three independent parameters to completely characterize the turbulence field, viz., U, M, and the viscosity $\nu = \kappa\,\mathrm{Pr}$, where Pr is the Prandtl number, and two independent parameters to completely characterize the source, namely, σ_o and x_o. On the other hand, since dispersion of the scalar plume is only dependent on the turbulence statistics at the source location, the relevant number of independent dimensional parameters required for simulating the dispersion from a single line source reduces to four and these can be taken as k_o, ε_o, σ_o, and κ (for a given Pr). Two length scales and two time scales that can be formed given the above four quantities are L_o, σ_o, T_o, and τ_κ, from which at most two independent nondimensional groups can be formed. In this work, we choose to work with the length scale ratio $\Lambda = \sigma_o/L_o$ and the Taylor scale Reynolds number R_λ.

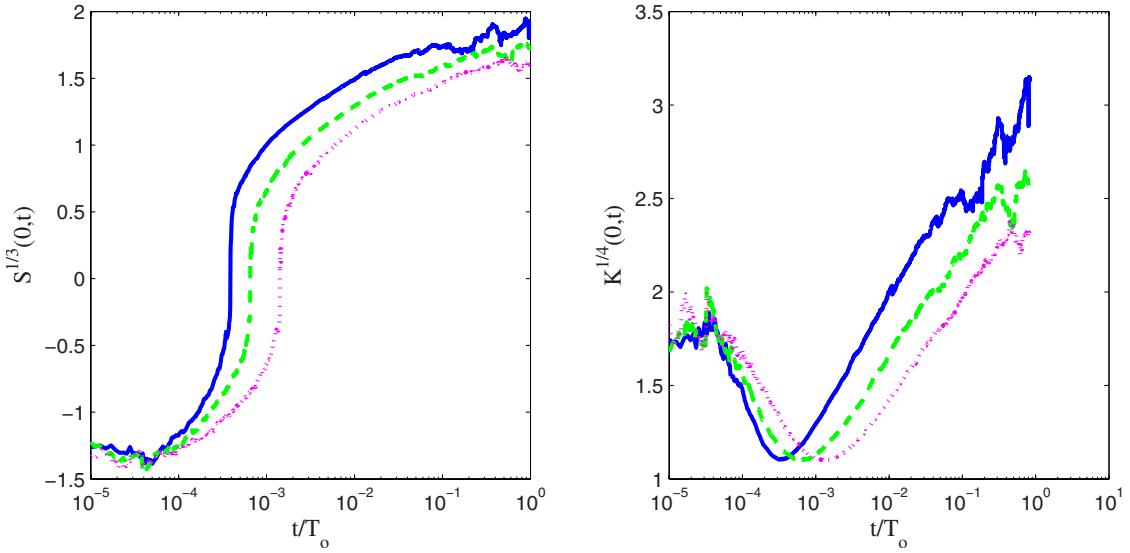

FIG. 24. (Color online) Skewness S and kurtosis K against flight time from the source for $\Lambda=1.3\times10^{-4}$ and different values of R_λ: $R_\lambda=750$ (solid line), $R_\lambda=400$ (dashed line), and $R_\lambda=250$ (dotted line).

In order to understand the effect of each of these nondimensional quantities on the evolution of the scalar field, the results from a set of five cases are presented for different combinations of Λ and R_λ. Both Λ and R_λ are chosen to vary by an order of magnitude. The value of Λ is typically chosen over the range of 5×10^{-5}–5×10^{-4}, whereas R_λ is chosen to vary between 100 and 1000. The details are summarized in Table IV.

Additionally, calculations are also performed for larger ranges in both $R_\lambda\sim70$–7000 and $\Lambda\sim2\times10^{-5}$–$2\times10^{-3}$ with an aim to study their effects on the centerline intensity of fluctuations. In particular, the maximum value $i_{\max}$ and the large-time asymptote i_∞ are analyzed in the Λ-R_λ space.

1. Dependence on the Reynolds number R_λ

As the first step, the dependence of various scalar statistics on R_λ is studied at a given value of Λ. The Langevin model constant C_0 is taken to be independent of R_λ and equal to 2.1. Figures 21–24 plot the centerline intensity of fluctuations, the normalized mean plume width, the normalized integral scalar variance, and higher moments of skewness and kurtosis, respectively, against flight time from the source for $\Lambda=1.3\times10^{-4}$ and for three different values of R_λ—250, 400, and 750.

Figure 21 displays an increase in the peak value of the centerline fluctuation intensity with an increase in R_λ. Additionally, the behavior at very early time ($t/T_o<3\times10^{-5}$) is independent of R_λ. Far downstream, again i seems to be independent of R_λ for a constant C_0 assumption. Figure 22 shows that the normalized mean plume width, σ_p/L_o, is independent of R_λ except at small times. Figure 23 compares the effect of R_λ on the evolution of the normalized integral scalar variance I. At very small times, I is independent of R_λ. Far downstream also, there is a similar trend. In the intermediate regime, the decay rate of the integral scalar variance is the same and is given by the slope of the curve, whereas R_λ has a direct effect on the magnitude. Figure 24 exhibits independence of the higher moments of the scalar from R_λ at very small times. For very large times, an increase in R_λ is equivalent to a shift of the plot to smaller t/T_o.

Second, i is analyzed further over a larger range of R_λ in terms of $i_{\max}$ and i_∞, which are the maximum value of i and the large-time asymptote, respectively. Figure 25 shows a

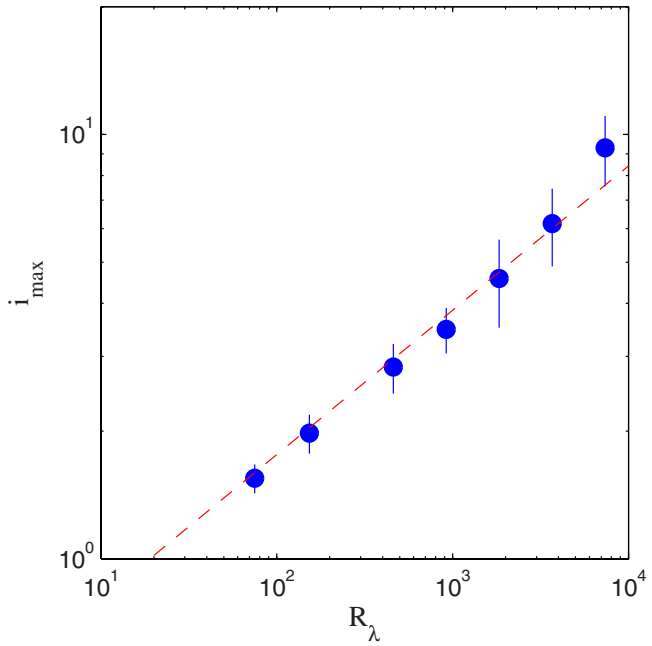

FIG. 25. (Color online) Maximum centerline intensity of fluctuation against R_λ for $\Lambda=1.3\times10^{-4}$. The solid lines indicate 95% confidence intervals. Dashed line of slope 1/3 is shown for reference.

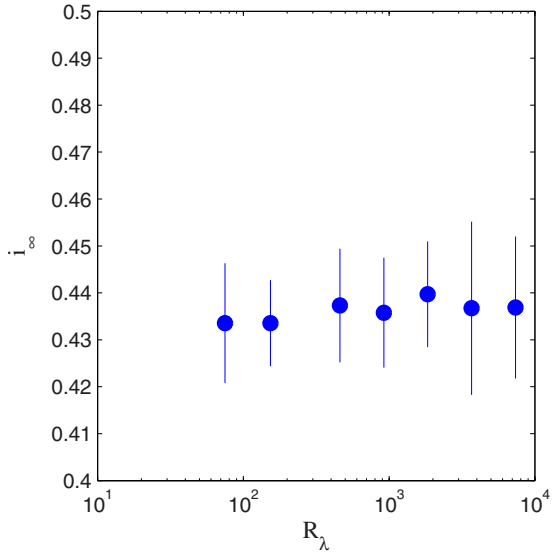

FIG. 26. (Color online) Estimate of the centerline intensity of fluctuation as $t \to \infty$ against R_λ for $\Lambda = 1.3 \times 10^{-4}$. The lines indicate 95% confidence intervals.

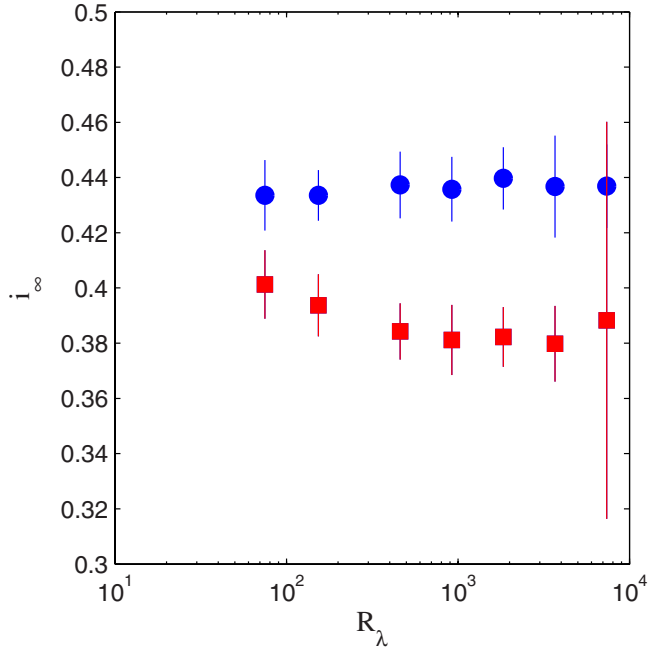

FIG. 28. (Color online) Estimate of the centerline intensity of fluctuation as $t \to \infty$ against R_λ for $\Lambda = 1.3 \times 10^{-4}$: $C_0 = 2.1$ (●) and $C_0(R_\lambda)$ (■). The lines indicate 95% confidence intervals.

log-log plot of i_{max} versus R_λ. In the range of R_λ considered, i_{max} varies approximately as $R_\lambda^{1/3}$ (as is shown by the dashed line) and does not appear to saturate to a constant level. Since, the scalar mean is not affected by R_λ for constant C_0, an increasing trend in i_{max} implies that the scalar fluctuations are increasing. Figure 26 is aimed at studying the effect of R_λ on i_∞ and as is evident from the plot, i_∞ is independent of R_λ.

Third, the effect on i_{max} and i_∞ of incorporating a R_λ dependence on C_0 is studied based on Pope.[12] Figure 27 compares i_{max} obtained under the assumption that $C_0 = 2.1$ with the estimates made incorporating the R_λ dependence of C_0. The estimates of i_{max} from the two approaches are within the 95% confidence intervals. Figure 28, however, shows some sensitivity to the value of C_0: including for the R_λ dependence of C_0 results in a decrease in i_∞ of no more than 10%.

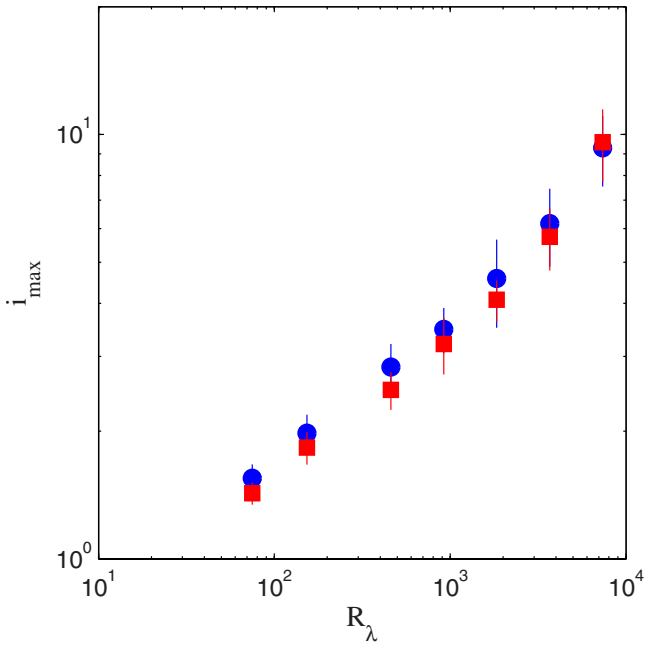

FIG. 27. (Color online) Maximum centerline intensity of fluctuation against R_λ for $\Lambda = 1.3 \times 10^{-4}$: $C_0 = 2.1$ (●) and $C_0(R_\lambda)$ (■). The lines indicate 95% confidence intervals.

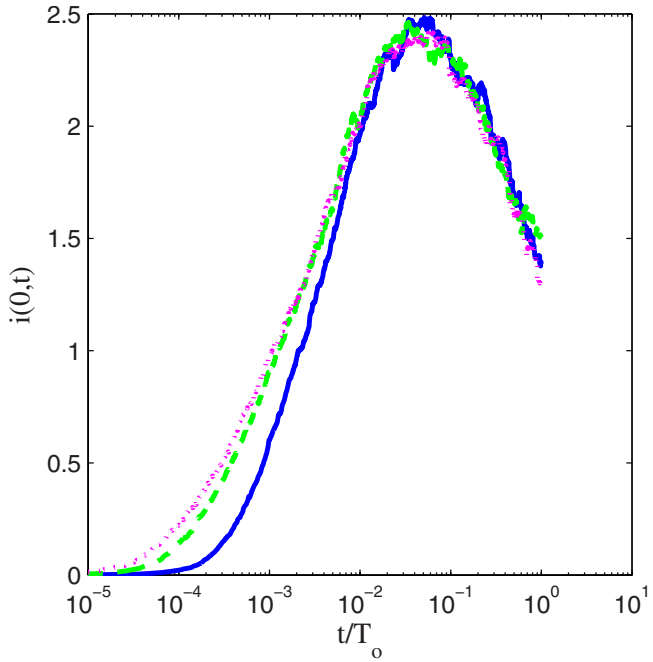

FIG. 29. (Color online) Centerline intensity of fluctuations, $i(0,t)$, vs flight time from the source at $R_\lambda = 400$ for different values of Λ: $\Lambda = 4.7 \times 10^{-4}$ (solid line), $\Lambda = 1.3 \times 10^{-4}$ (dashed line), and $\Lambda = 5.8 \times 10^{-5}$ (dotted line).

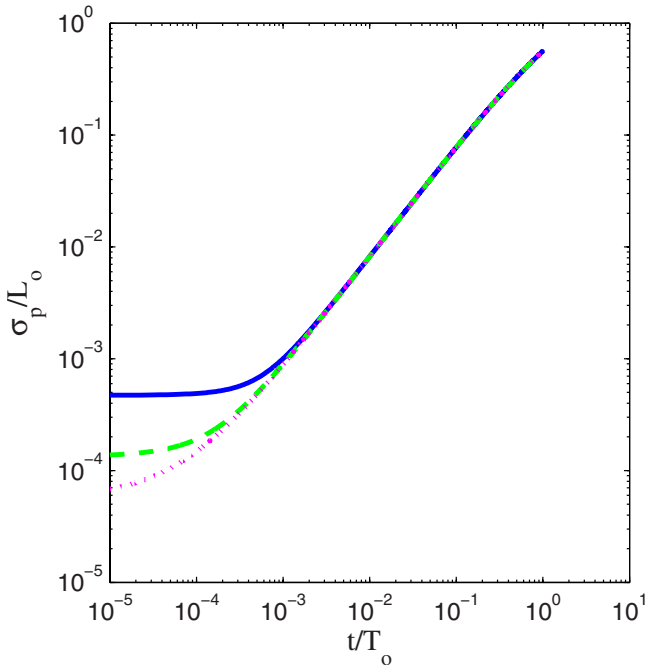

FIG. 30. (Color online) Mean plume width normalized by the turbulence integral scale at the source, L_o, against flight time from the source at $R_\lambda = 400$ for different values of Λ: $\Lambda = 4.7 \times 10^{-4}$ (solid line), $\Lambda = 1.3 \times 10^{-4}$ (dashed line), and $\Lambda = 5.8 \times 10^{-5}$ (dotted line).

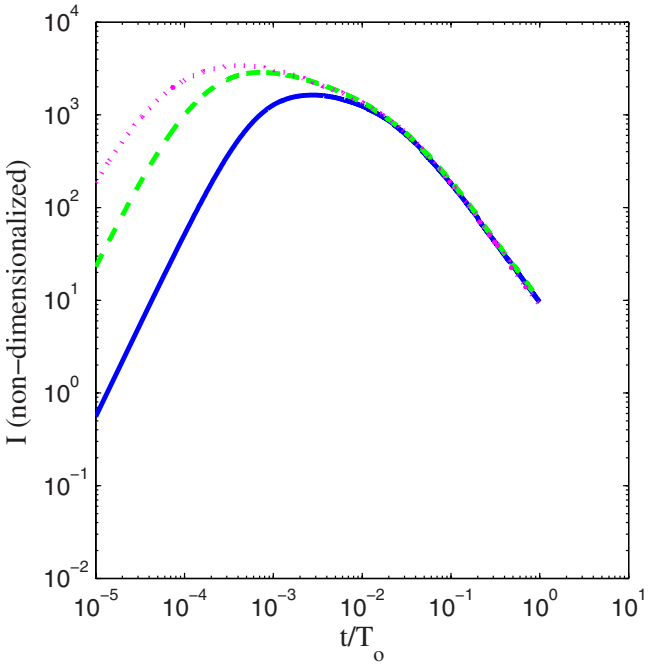

FIG. 31. (Color online) Integral of scalar variance, I, normalized by $2\pi L_o/Q^2$ against flight time from the source at $R_\lambda = 400$ for different values of Λ: $\Lambda = 4.7 \times 10^{-4}$ (solid line), $\Lambda = 1.3 \times 10^{-4}$ (dashed line), and $\Lambda = 5.8 \times 10^{-5}$ (dotted line).

2. Dependence on normalized source size Λ

Next, the effect of $\Lambda = \sigma_o/L_o$ on the scalar field is studied at a constant value of R_λ of 400. As in Sec. V F 1, the centerline intensity of fluctuations, mean plume width, integral scalar variance, skewness, and kurtosis are probed to understand the effect of Λ on the scalar field.

Figure 29 plots the centerline intensity of fluctuations against flight time from the source for three different values of Λ, 5.8×10^{-5}, 1.3×10^{-4}, and 4.7×10^{-4}. Except for the effect of the variation in Λ at very early times, there is little dependence of i on Λ. Similar trends are observed in Fig. 30 for the normalized mean plume width, σ_p/L_o, in Fig. 31 for the normalized integral scalar variance I, and in Fig. 32 for skewness and kurtosis.

Since Λ affects the various scalar statistics only at very small times close to the source, each of the quantities can be appropriately scaled to make them independent of Λ. The effect of the source size on the mean plume width is purely an additive effect as is evident from Eq. (11) and therefore, $(\sigma_p^2 - \sigma_o^2)/L_o$ is independent of Λ. Figure 33 confirms this observation.

Moreover, the centerline intensity of fluctuations, i, at very small times can be analytically obtained using the laminar thermal wake modeling approach to be

$$i(0,t) = \sqrt{\frac{G^2+1}{\sqrt{2G^2+1}}} - 1, \tag{67}$$

where

$$G(t) = \left(\frac{\sigma_{v_o}^2 T_o}{2\kappa}\right)\left[\frac{t^2}{T_o\left(t + \frac{1}{2}\tau_\kappa\right)}\right]. \tag{68}$$

Since i is a function of G only at very small times, accurate calculations of i can be expected to scale as G does at small times. Figure 34 shows the plot of i against $t^2/[T_o(t + \tau_\kappa/2)]$ both in linear-log scale and log-log scale, thereby effectively eliminating the influence of Λ on i. Figures 35 and 36 plot $i_{\max}$ and i_∞, respectively, over a larger range of Λ at $R_\lambda = 460$. Both the figures show no sensitivity to Λ (at least for $\Lambda \leq 10^{-3}$), strengthening the conclusion earlier from this section that Λ affects the statistics only at very early times.

VI. CONCLUSIONS

Detailed PDF calculations have been performed of the dispersion from line sources in grid turbulence. The PDF method uses the modified IECM mixing model, which is summarized in Sec. III E. The model calculations are primarily compared with the experiments of Warhaft[7] and the IECM model calculations of Sawford[23] for single and pairs of line sources. An extension is also made to simulate an array of four line sources and heated mandolines.

Due to the disparity in the length scales of the plume and turbulent energy-containing motions very close to the source, the effects of molecular diffusion have to be accounted for in

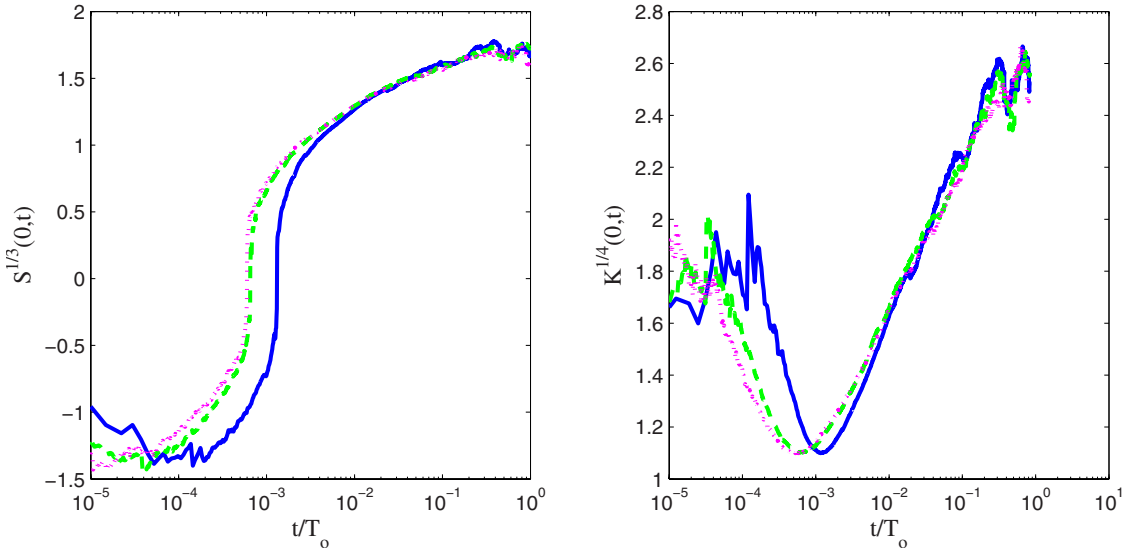

FIG. 32. (Color online) Skewness S and kurtosis K against flight time from the source at $R_\lambda=400$ for different values of Λ: $\Lambda=4.7\times10^{-4}$ (solid line), $\Lambda=1.3\times10^{-4}$ (dashed line), and $\Lambda=5.8\times10^{-5}$ (dotted line).

the scalar evolution equation. However, modeling the molecular diffusion as a random walk in the evolution equation for particle displacement in conjunction with the IECM mixing model gives rise to a spurious production term in the scalar variance transport equation. The spurious production term is avoided by instead incorporating the effects of molecular diffusion directly into the IECM mixing model by the addition of a conditional scalar drift term.

Modeling the instantaneous plume as a laminar thermal wake provides a model for the evolution of the mixing rate very close to the source. This small-time asymptote, $\omega_m^0(t)$, Eq. (51), provides a nongeneral model for the early time behavior of the mixing time scale. Far away from the source, all memory about the initial source conditions is lost and the mechanical-to-scalar time scale ratio eventually asymptotes to a constant as determined by various DNS studies. Hence, the large-time asymptote of the mixing rate $\omega_m^\infty(t)$ is retained to be proportional to the turbulence rate ε/k. The new mixing rate specification used here is simply a blending of the two asymptotic expressions, which is correct in both the limits, $\omega_m=\omega_m^0$ at $t=0$ and $\omega_m\to\omega_m^\infty$ as $t\to\infty$.

The above mentioned mixing rate involves only one adjustable parameter, that being the time scale ratio C_ϕ. Even though the proposed time scale was derived from the transport equation of the integral mean square of the scalar, model calculations using this time scale not only predict different statistics correctly on the plume centerline but also the radial profiles at different stages in the development of the plume, including higher moments, skewness, and kurtosis, for which comparisons are made with the experimental data of Sawford and Tivendale reported by Sawford[23] and with the previous calculations of Sawford[23] for the single line source.

The PDF model is applied to a pair of line sources and an array of four line sources and is shown to perform well in comparison to the experimental data. The cross-correlation coefficient between any pair of sources gives an indication of the extent of flapping of the wake and interwake interferences. These accurate predictions suggest that the effects of molecular diffusion have been incorporated accurately. The modified IECM model is also tested to verify the dependence of the scalar variance decay rate on the distance between the sources in the mandoline with respect to the integral turbulence length scale.[6] The present calculations agree with the experimental data of Warhaft and Lumley[6] and are consistent

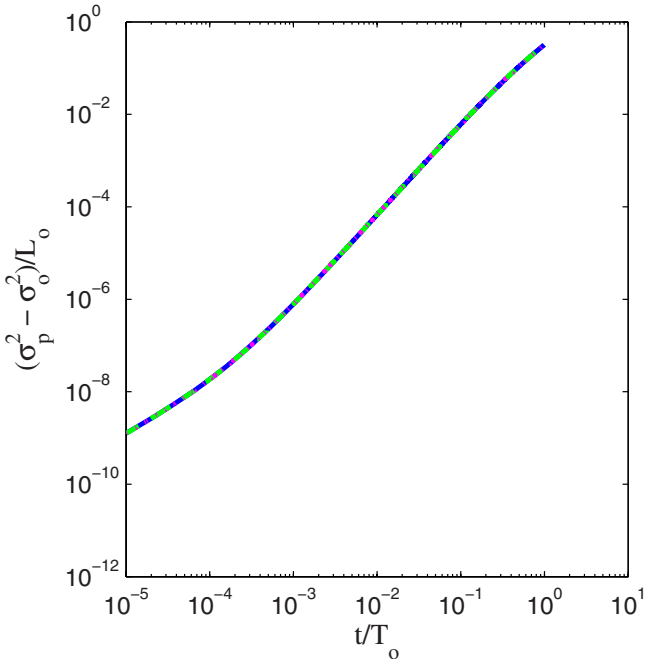

FIG. 33. (Color online) Normalized mean plume width minus the effect of the source plotted against flight time from the source at $R_\lambda=400$ for different values of Λ: $\Lambda=4.7\times10^{-4}$ (solid line), $\Lambda=1.3\times10^{-4}$ (dashed line), and $\Lambda=5.8\times10^{-5}$ (dotted line). (The lines are indistinguishable.)

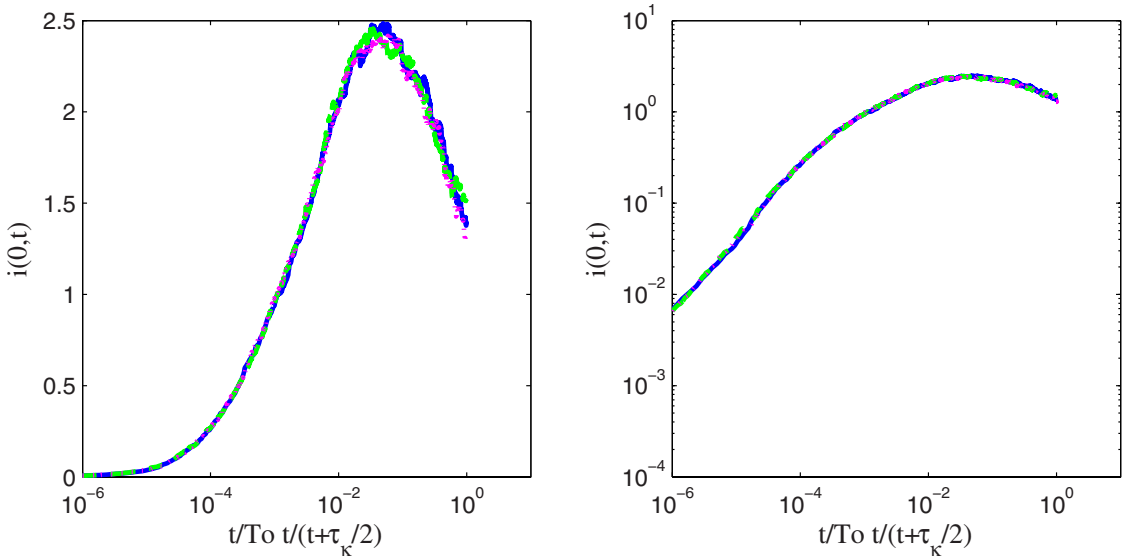

FIG. 34. (Color online) Centerline intensity of fluctuations, $i(0,t)$, vs time, $\bar{t}=t^2/[T_o(t+\tau_\kappa/2)]$, at $R_\lambda=400$ for different values of Λ: $\Lambda=4.7\times10^{-4}$ (solid line), $\Lambda=1.3\times10^{-4}$ (dashed line), and $\Lambda=5.8\times10^{-5}$ (dotted line). (The lines are indistinguishable.)

with the observations of Sreenivasan *et al.*[29] which show that, at distances far downstream from the mandoline, the scalar variance decay rate is independent of the length scale ratio (when plotted against distance from the mandoline).

The choices of standard values for the model parameters, $C_0=2.1$ and $C_\phi=1.5$, compare well with the experimental observations. Additionally, dispersion from a single line source is studied in greater detail over a range of the parameter space. The effect of the source size is only significant at very small times from the source, whereas with a constant C_0 assumption, the effects of Reynolds numbers are evident only at intermediate times. The large-time asymptote of the centerline intensity of fluctuations tends to a constant (approximately 0.4) independent of both the nondimensional source size and Reynolds numbers for the range of parameter space explored, while the maximum value of the centerline fluctuation intensity shows a dependence on the Reynolds number (approximately as $R_\lambda^{1/3}$) but not on the source size. Data from experiments and/or DNS are required to corroborate the model predictions at large Reynolds numbers.

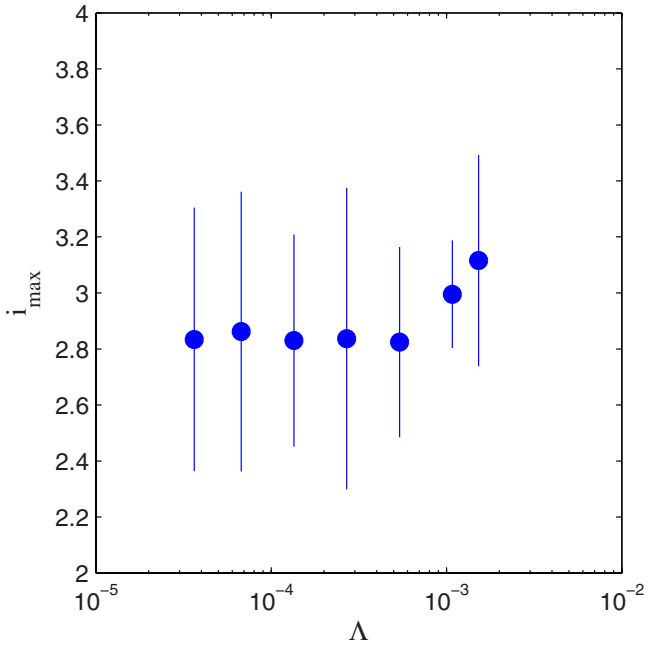

FIG. 35. (Color online) Maximum centerline intensity of fluctuation against Λ for $R_\lambda=460$. The lines indicate 95% confidence intervals.

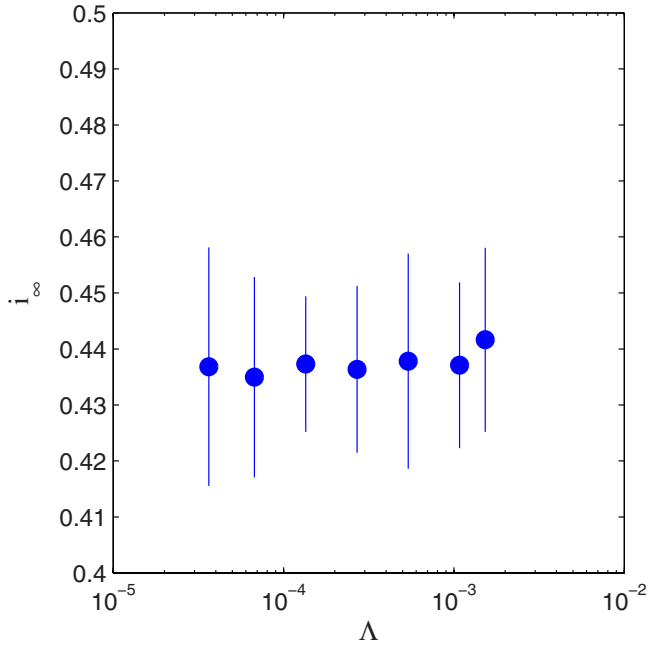

FIG. 36. (Color online) Estimate of the centerline intensity of fluctuation as $t\to\infty$ against Λ for $R_\lambda=460$. The lines indicate 95% confidence intervals.

ACKNOWLEDGMENTS

This paper is dedicated to John Kim on the occasion of his 60th birthday. S.V. would like to thank Professor Z. Warhaft and Brian Sawford for valuable comments and also Prasad Bhave and Haifeng Wang for insightful discussions during the course of this work. This research is supported by the Department of Energy under Grant No. DE-FG02-90ER. This research was conducted using the resources of the Cornell University Center for Advanced Computing, which receives funding from Cornell University, New York State, the National Science Foundation, and other leading public agencies, foundations, and corporations.

[1] G. I. Taylor, "Diffusion by continuous movements," Proc. London Math. Soc. **20**, 196 (1922).
[2] G. I. Taylor, "Statistical theory of turbulence IV: Diffusion in a turbulent air stream," Proc. R. Soc. London, Ser. A **151**, 465 (1935).
[3] M. S. Uberoi and S. Corrsin, "Diffusion of heat from a line source in isotropic turbulence," National Aeronautics and Space Administration Report No. 1142, 1953.
[4] A. A. Townsend, "The diffusion behind a line source in homogeneous turbulence," Proc. R. Soc. London, Ser. A **224**, 487 (1954).
[5] H. Stapountzis, B. L. Sawford, J. C. R. Hunt, and R. E. Britter, "Structure of the temperature field downwind of a line source in grid turbulence," J. Fluid Mech. **165**, 401 (1986).
[6] Z. Warhaft and J. L. Lumley, "An experimental study of the decay of temperature fluctuations in grid-generated turbulence," J. Fluid Mech. **88**, 659 (1978).
[7] Z. Warhaft, "The interference of thermal fields from line sources in grid turbulence," J. Fluid Mech. **144**, 363 (1984).
[8] Z. Warhaft, "The use of dual heat injection to infer scalar covariance decay in grid turbulence," J. Fluid Mech. **104**, 93 (1981).
[9] S. B. Pope, "Transport equation for the joint probability density function of velocity and scalars in turbulent flow," Phys. Fluids **24**, 588 (1981).
[10] S. B. Pope and Y. L. Chen, "The velocity dissipation probability density function model for turbulent flows," Phys. Fluids A **2**, 1437 (1990).
[11] S. B. Pope, "Application of the velocity dissipation probability density function model to inhomogeneous turbulent flows," Phys. Fluids A **3**, 1947 (1991).
[12] S. B. Pope, "Lagrangian PDF methods for turbulent flows," Annu. Rev. Fluid Mech. **26**, 23 (1994).
[13] J. Villermaux and J. C. Devillon, "Représentation de la coalescence et de la redispersion des domaines de ségrégation dans un fluide par un modèle d'interaction phénoménologique," in *Proceedings of the Second International Symposium on Chemical Reaction Engineering* (Elsevier, New York, 1972), pp. 1–13.
[14] C. Dopazo and E. E. O'Brien, "An approach to the autoignition of a turbulent mixture," Acta Astronaut. **1**, 1239 (1974).
[15] S. B. Pope, "PDF methods for turbulent reactive flows," Prog. Energy Combust. Sci. **11**, 119 (1985).
[16] R. L. Curl, "Dispersed phase mixing I," AIChE J. **9**, 175 (1963).
[17] J. C. Song, "A velocity-biased turbulent mixing model for passive scalars in homogeneous turbulence," Phys. Fluids **30**, 2046 (1987).
[18] S. B. Pope, "On the relationship between stochastic Lagrangian models of turbulence and second-moment closures," Phys. Fluids **6**, 973 (1994).
[19] R. O. Fox, "On velocity conditioned scalar mixing in homogeneous turbulence," Phys. Fluids **8**, 2678 (1996).
[20] M. Overholt and S. B. Pope, "Direct numerical simulations of a passive scalar with imposed mean gradient in isotropic turbulence," Phys. Fluids **8**, 3128 (1996).
[21] S. B. Pope, "The vanishing effect of molecular diffusivity on turbulent dispersion: Implications for turbulent mixing and the scalar flux," J. Fluid Mech. **359**, 299 (1998).
[22] M. S. Anand and S. B. Pope, "Diffusion behind a line source in grid turbulence," in *Turbulent Shear Flows 4*, edited by L. J. S. Bradbury, F. Durst, B. E. Lauder, F. W. Schmidt, and J. H. Whitelaw (Springer-Verlag, Berlin, 1985), p. 46.
[23] B. Sawford, "Micro mixing modeling of scalar fluctuations for plumes in homogeneous turbulence," Flow, Turbul. Combust. **72**, 133 (2004).
[24] A. Luhar and B. L. Sawford, "Micro-mixing modeling of concentration fluctuations in inhomogeneous turbulence in the convective boundary layer," Boundary-Layer Meteorol. **114**, 1 (2005).
[25] B. Sawford, "Conditional scalar mixing statistics in homogeneous isotropic turbulence," New J. Phys. **6**, 55 (2004).
[26] G. Brethouwer and F. T. M. Nieuwstadt, "DNS of mixing and reaction of two species in a turbulent channel flow: A validation of the conditional moment closure," Flow, Turbul. Combust. **66**, 209 (2001).
[27] V. Eswaran and S. B. Pope, "Direct numerical simulations of the turbulent mixing of a passive scalar," Phys. Fluids **31**, 506 (1988).
[28] A. Juneja and S. B. Pope, "A DNS study of turbulent mixing of two passive scalars," Phys. Fluids **8**, 2161 (1996).
[29] K. R. Sreenivasan, S. Tavoularis, R. Henry, and S. Corrsin, "Temperature fluctuations and scales in grid-generated turbulence," J. Fluid Mech. **100**, 597 (1980).
[30] B. Sawford and J. C. R. Hunt, "Effects of turbulence structure, molecular diffusion and source size on scalar fluctuations in homogeneous turbulence," J. Fluid Mech. **165**, 373 (1986).
[31] M. S. Borgas and B. L. Sawford, "Molecular diffusion and viscous effects on concentration statistics in grid turbulence," J. Fluid Mech. **324**, 25 (1996).
[32] D. Livescu, F. A. Jaberi, and C. K. Madnia, "Passive-scalar wake behind a line source in grid turbulence," J. Fluid Mech. **416**, 117 (2000).
[33] R. McDermott and S. B. Pope, "A particle formulation for treating differential diffusion in filtered density function methods," J. Comput. Phys. **226**, 947 (2007).
[34] T. D. Dreeben and S. B. Pope, "Probability density function/Monte Carlo simulation of near wall turbulent flows," J. Fluid Mech. **357**, 141 (1998).
[35] S. B. Pope, *Turbulent Flows* (Cambridge University Press, Cambridge, 2000).
[36] M. Cassiani, P. Franzese, and U. Giostra, "A PDF micromixing model of dispersion for atmospheric flow. Part I: Development of the model, application to homogeneous turbulence and to neutral boundary layer," Atmos. Environ. **39**, 1457 (2005).
[37] It is to be noted that for the IECM model there exists a mixing rate which yields the correct evolution of the integral scalar variance. But the modified IECM model, in addition to predicting the correct evolution of the integral scalar variance, also yields scalar variance profiles that are in agreement with the laminar thermal wake model at early times (whereas the unmodified IECM model does not).